A STATISTICAL ANALYSIS OF COLD WAKE FORMATION WITH IMPLICATIONS FOR CLIMATE AND TROPICAL CYCLONE INTENSITY

A Thesis

by

Robert Joseph Haslett

Submitted to the Graduate and Professional School of
Texas A&M University
in partial fulfillment of the requirements for the degree of

MASTER OF SCIENCE

Chair of Committee,	Henry Potter
Committee Members,	Steve DiMarco
	Ramalingam Saravanan
Head of Department,	Shari Yvon-Lewis

May 2023

Major Subject: Oceanography

ABSTRACT

Tropical cyclones (TCs) are dangerous weather events that cause significant damage to infrastructure and loss of life each year. TC track forecasting has improved considerably in recent decades, though improvements to intensity forecasts are not as significant. TCs gain energy through heat fluxes from warm ocean waters into the atmosphere. Cold wakes are trails of cooler waters observed beneath TCs that mitigate intensification by reducing these fluxes. This study uses TC data from Colorado State University, oceanic profile data from Argo floats, and satellite sea surface temperature data from NASA to quantify the parameters contributing to hurricane-induced oceanic cooling (ΔSST) in the North Atlantic Ocean. Results indicate that hurricane translation speed and minimum sea level pressure are the best predictors of ΔSST, followed by oceanic isothermal layer depth. A well-rounded knowledge of cold wakes is critical to better understanding TC intensity and ultimately improving the accuracy of TC intensity forecasts.

ACKNOWLEDGEMENTS

First and foremost, I would like to express thanks to my committee chair, Dr. Henry Potter, for his guidance and support over the past two years. I am grateful to have had the opportunity to work closely with and learn from him as a mentee, student, and collaborator. His knowledge, expertise, and feedback were paramount in helping me traverse the challenges of this project while furthering my computational, analytical, and research skills.

I am also grateful for my committee members, Dr. Steve DiMarco and Dr. Ramalingam Saravanan, for their support and feedback. Their comments and suggestions were pivotal in helping me refine my research questions and explore new ideas that were key to the completion of this project. I am also thankful to Dr. Chrissy Wiederwohl for her guidance in helping me navigate the program and answering countless questions I had along the way.

I would also like to thank my peers in the department for always supporting me and making my time at Texas A&M University a truly memorable experience. In addition to being friends, many also served as mentors, from helping me think through complex research questions to navigating graduate school in general, and to that I am grateful.

Lastly, I am thankful to my family and friends for their unwavering support and encouragement over the past two years. Their love and support gave me the motivation to persevere through the highs and lows and I could not have done this without them.

CONTRIBUTORS AND FUNDING SOURCES

Contributors

This project was supervised by a thesis committee consisting of Dr. Henry Potter (Thesis Advisor and Committee Chair) of the Department of Oceanography, Dr. Steve DiMarco (Committee Member) of the Department of Oceanography, and Dr. Ramalingam Saravanan (Committee Member) of the Department of Atmospheric Sciences.

Funding Sources

Graduate study and research funding was provided by the Department of Oceanography and the College of Arts & Sciences at Texas A&M University.

NOMENCLATURE

AEW	African Easterly Wave
ANOVA	Analysis of Variance
AOML	Atlantic Oceanographic and Meteorology Laboratory
AVHRR	Advanced Very High Resolution Radiometer
BGC	Biogeochemical
BLT	Barrier Layer Thickness
CO_2	Carbon Dioxide
CSU	Colorado State University
CTD	Conductivity, Temperature, Depth
DAC	Data Acquisition Center
EBTRK	Extended Best Track Dataset
GDAC	Global Data Assembly Center
GHRSST	Group for High Resolution Sea Surface Temperature
GHG	Greenhouse Gas
HURDAT2	Best Track Dataset
IPLD	Isopycnal Layer Depth
ITLD	Isothermal Layer Depth
JPL	Jet Propulsion Laboratory
MLD	Mixed Layer Depth
MLR	Multilinear Regression
MODIS	Moderate Resolution Imaging Spectroradiometer
MUR	Multi-scale Ultra-high Resolution
NASA	National Aeronautics and Space Administration
NHC	National Hurricane Center
NOAA	National Oceanic and Atmospheric Administration
PCA	Principal Component Analysis
PhOD	Physical Oceanography Division

PSU	Practical Salinity Units
QC	Quality Control
RMW	Radius of Maximum Winds
SSHWS	Saffir-Simpson Hurricane Wind Scale
SST	Sea Surface Temperature
SSTA	Sea Surface Temperature Anomaly
TC	Tropical Cyclone
TCHP	Tropical Cyclone Heat Potential
TCOP	Tropical Cyclone Observation Point

TABLE OF CONTENTS

LIST OF FIGURES

Page

LIST OF TABLES

Page

1. INTRODUCTION

1.1 Tropical Cyclones

1.1.1 Overview of Tropical Cyclones

Tropical cyclones (TCs) are powerful weather systems that can develop in several ocean basins around the world, and they are known by different names throughout these basins. TCs that develop in the North Atlantic and Northeast Pacific are referred to as hurricanes. In the Northwest Pacific they are called typhoons, and in the South Pacific and Indian Oceans, they are called cyclones (Shultz et al., 2005). The area of interest for this project is the North Atlantic basin, so the terms tropical cyclone, TC, and hurricane will be used interchangeably.

Per their name, TCs are storms that form over the warm ocean waters of the tropics and exhibit cyclonic rotation. Two notable features of TCs include a warm core and a low central pressure (Emanuel, 2003). Air moves from areas of high pressure to low pressure, so air masses around these systems are directed inwards. The cyclonic rotations of a TC's wind field is a product of the Coriolis force that results from the rotation of the Earth. The Coriolis force causes fluids in motion to divert to the right in the Northern Hemisphere and to the left in the Southern Hemisphere. Because of this, TC's experience counterclockwise winds in the Northern Hemisphere and clockwise winds in the Southern Hemisphere.

1.1.2 Origin and Genesis

The majority of hurricanes that develop over the North Atlantic arise from atmospheric disturbances that originate over Africa and travel west into the basin. These disturbances, commonly known as African Easterly Waves (AEWs), were the source of 75% of North Atlantic

hurricanes in 1994 and 91% in 1995 (Pasch et al., 1998). The mechanisms that allow for AEWs to form are complex, but the main contributing factor is the presence of baroclinic and barotropic instabilities within the African Easterly Jet during summer months (Thorncroft & Hoskins, 1994). As these disturbances propagate west, they must meet a set of ideal conditions to undergo hurricane genesis. One condition is warm sea surface temperature (SSTs) beneath the disturbance. The role of SST for genesis is pivotal as hurricanes are fueled by the large latent and sensible heat fluxes associated with warm ocean waters (Kanada et al., 2017). Prior studies have put forth a threshold of 26 °C SSTs, below which genesis could not be maintained due to lack of fuel in the form of heat energy (Palmen, 1948; D'Asaro et al., 2007).

An atmospheric parameter that can disrupt hurricane genesis is vertical wind shear. A region experiencing low vertical wind shear has similar wind speeds and directions throughout the atmospheric column. Conversely, regions with high vertical wind shear see significant changes in wind speed and direction at varying altitudes. For genesis, ideal conditions are those in which vertical wind shear is minimal (Gray, 1975). Under these circumstances, heat uptake into the upper atmosphere continues relatively undisturbed allowing for the cyclone to maintain structure and intensify. When vertical wind shear is great, this process is disrupted and the vertical structure of the cyclone is likely to degrade. The amount of vertical wind shear present is particularly critical in the early stages of genesis as less developed cyclones are more vulnerable to its effects (Frank & Ritchie, 2001).

A third condition important for hurricane genesis is that the system stays within the latitudinal bounds that favor cyclonic rotation. As previously mentioned, the Coriolis force brought on by the rotation of the Earth directs airflow to the right in the Northern Hemisphere and to the left in the Southern Hemisphere. Because it is a product of Earth's rotation, the

Coriolis force is a function of latitude, and can be expressed in the equation for the Coriolis parameter *f*:

$$f = 2\Omega sin(\varphi)$$

where Ω is the rotation of the Earth and is equal to 7.27×10^{-5} rad s^{-1}, and φ is latitude in degrees. From this equation, it can be observed that the impact of the Coriolis force increases with latitude, and is not present at the equator where φ (and subsequently *f*) are equal to zero. It has been surmised that a latitude of at least 5° is necessary for the Coriolis force to be strong enough to support the cyclonic rotation of a disturbance (Gray, 1975).

1.1.3 Structure

Every hurricane is unique, but there are several structural characteristics that many have in common. One such characteristic is the presence of an eye, which is an area of relatively calm conditions, warm temperatures, and low pressures located near the center of the system (Smith, 1980). There are several theories as to how the eye forms, but each come down to a combination of pressure gradients, the Coriolis force, convection, and the vertical movement of air near the hurricane center. The foundation of a hurricane is an area of low pressure, and air pressure gradients result in high pressure air moving inward toward this low pressure center. The inward movement of air, in conjunction with the Coriolis force, results in cyclonic rotation centered around the origin of low pressure. At some distance from the hurricane center, these cyclonic winds foster a continual upward movement of air, compounding the decreasing pressure at lower altitudes and creating a region of high pressure at upper altitudes. This region of high pressure often exhibits anticyclonic rotation as air moves outward and is deflected by the Coriolis force. However, some of this air is instead directed back inward where it builds up, increases pressure,

and travels back down the center of the storm, working to create a region of minimal rain and relative calm known as the eye (Vigh, 2010).

Surrounding the eye is a structure known as the eyewall, which is the region of the storm associated with the heaviest precipitation and the greatest intensities. Further out from the eyewall are a series of large convective clouds known as rainbands that migrate inwards towards the eyewall over time (Houze Jr. et al., 2007). In powerful hurricanes, as these rainbands develop and move inward, the eyewall begins to fall apart, at which points the storm weakens. Over 24 to 48 hours, these rainbands can entirely take over the eyewall in a process known as an eyewall replacement cycle (Sitkowski et al., 2011). At this stage, there is a new well-structured eyewall and the storm can begin to regain intensity if other conditions are favorable.

1.1.4 Movement

The zonal and meridional movements of hurricanes are grouped into two categories: environmental steering and beta drift. Of the two, environmental steering is the leading mechanism for hurricane movement (Galarneau & Davis, 2013). The primary factor in relation to environmental steering is the speed and direction of regional wind patterns in the atmospheric column. Though these wind patterns differ with altitude, those at the 700 to 500 mbar level provide the best predictions for hurricane movement (Chan & Gray, 1982). In the North Atlantic, hurricanes are generally guided to the west by easterly trade winds.

The second mechanism controlling hurricane movement is beta drift. A North Atlantic hurricane, for example, exhibits counterclockwise airflow at lower altitudes, fostering positive relative vorticity (Chan, 1982). On the western side of this hurricane, airflow is traveling towards the equator, subsequently decreasing planetary vorticity. As a result, the relative vorticity of the

hurricane increases to compensate. The opposite occurs on the eastern side of the hurricane. Airflow is poleward, increasing planetary vorticity resulting in a decrease in the relative vorticity. Hurricanes are predisposed to move towards areas where relative vorticity is increasing, thus resulting in an additional westward propagation. Furthermore, in the Northern Hemisphere, counterclockwise flow on the western side where relative vorticity is positive and clockwise flow on the eastern side where relatively vorticity is negative result in a channel that directs air northward from the center of the system. These two effects combine to produce the phenomenon of beta drift, causing hurricanes to propagate poleward and to the west.

1.2 Cold Wakes

1.2.1 Overview of Cold Wakes

During the life of a hurricane, several oceanic and atmospheric factors contribute to a cooling of the upper ocean. These signatures of relatively cooler waters left in the paths of hurricanes are called cold wakes (Figure 1). There are several processes responsible for the oceanic cooling observed beneath hurricanes, one being vertical mixing and entrainment. Powerful winds within hurricanes transfer momentum into the sea surface, generating vertical mixing at the top of the water column. This vertical mixing results in the entrainment of cooler waters from beneath the thermocline into the mixed layer (Yablonsky & Ginis, 2012), leading to both a deepening and cooling of the mixed layer beneath the hurricane (Ginis, 2002).

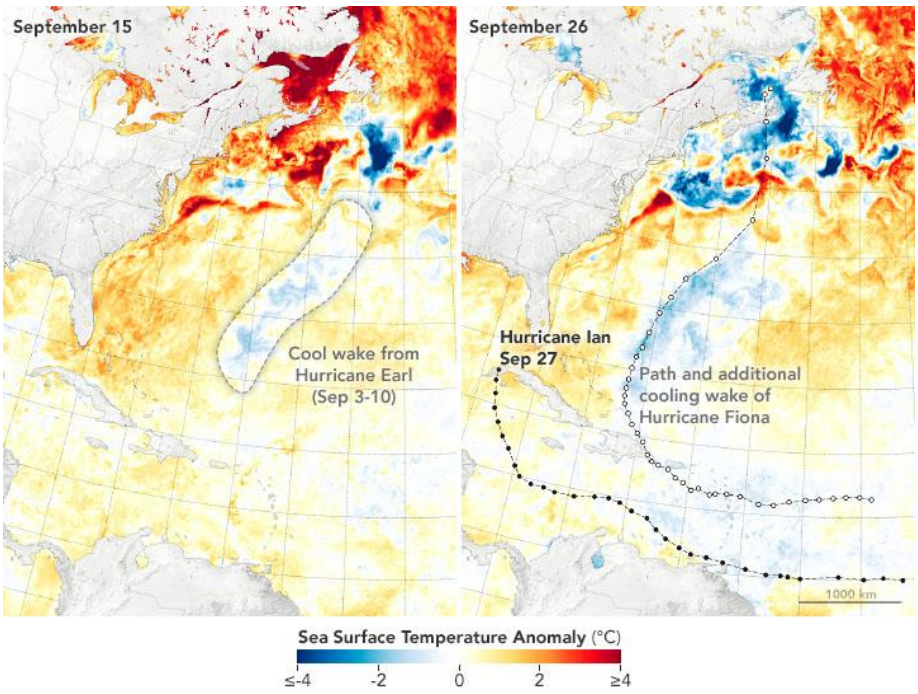

Figure 1: Daily SSTAs in the North Atlantic Ocean from September 15th (left) and September 26th (right), 2022. Warm colors indicate higher than average SSTs and cold colors indicate colder than average SSTs. Image made by Joshua Stevens, NASA Earth Observatory.

A second process that contributes to the oceanic cooling is upwelling. There are two mechanisms by which upwelling occurs beneath hurricanes, the first relating to wind direction and the Coriolis force. Cyclonic winds present within hurricanes often result in cyclonic surface currents beneath the storm. These surface currents are then deflected away from the hurricane center due to the Coriolis force, leading to the upwelling of cooler waters from below to replace those that have been deflected. The second mechanism, known as the inverse barometer effect, relates to pressure differences between the hurricane center and outer parts of the hurricanes. Because of the relatively low pressures at the hurricane center, waters there are not held down as much in comparison to outer parts of the storm where the atmospheric pressure at the air-sea interface in higher. This results in a bulging of waters beneath the low pressure center which then flow downhill towards the perimeter of the hurricane. A 1 mbar decrease in atmospheric pressure

at the air sea interface can result in a 1 cm increase in sea surface height (Murty & Neralla, 1992). Waters flowing away from the hurricane center are then replaced with the upwelling of cooler waters from beneath the thermocline. The upwelling of these cooler waters from both of these processes often causes the oceanic mixed layer to shoal which further enhances entrainment by minimizing the vertical distance that waters need to be mixed in order for entrainment to occur (Greatbatch, 1985).

Air-sea fluxes, principally latent and sensible heat fluxes, also contribute to cold wake development (e.g., Price, 1981; Potter et al., 2017). The contribution of these fluxes to oceanic cooling is relatively minor (~10% of total cooling) compared to vertical mixing and upwelling. The latent heat flux, also referred to as a moisture flux, is associated with the transfer of energy between the ocean and atmosphere via phase changes of water molecules (e.g., evaporation). Heat energy is required for water molecules to evaporate from the ocean into the atmosphere. As such, the evaporation of surface waters which help fuel the hurricanes also result in a cooling of the sea surface from the same transfer of heat energy. The sensible heat flux relates to air-sea energy transfers through a combination of conduction and convection. During the warmer months of hurricane season, SSTs tend to be larger than air temperatures at the air-sea interface, which is the principal cause of heat fluxes between the two mediums.

The cooling, spatial structure, and temporal evolution of cold wakes varies depending on local and regional conditions. Cooling can be less than 1 °C (Cione & Uhlhorn, 2003) or up to 10 °C as observed under Typhoon Kai-Tak (2000) (Chiang et al., 2011). The greatest cooling typically occurs within the first few days of a hurricane's passing, at which point the upper ocean begins a gradual return to pre-hurricane conditions (Mei & Pasquero, 2013). This exponential return of SSTs is confirmed by an analysis of North Atlantic hurricanes which revealed that

roughly 80% of oceanic cooling at the sea surface subsides after 20 days, with almost 100% subsiding after 60 days (Haakman et al., 2019). Although the return of the upper ocean to pre-hurricane conditions typically takes a couple weeks, under late-season hurricanes, oceanic conditions may not return to pre-hurricanes levels for several months (Potter et al., 2017).

The location of greatest cooling is typically observed to the right of the hurricane track in the Northern Hemisphere, and left-of-track in the Southern Hemisphere (Jordan & Frank, 1964). There are two mechanisms that cause this, one being the clockwise rotation of the wind stress vector right-of-track coinciding with the rotation of inertial currents within the mixed layer resulting in a resonation and amplification of vertical mixing and subsequent cooling (Gonella, 1972). The other mechanism is the presence of larger, more powerful waves located in the front-right quadrant relative to the hurricane track which transfer momentum deeper into the mixed layer, enhancing mixing (Collins III et al., 2018).

1.2.2 Development

Cold wake development is controlled by both oceanic and atmospheric conditions to varying degrees. One notable atmospheric contributor is storm strength, frequently defined as a function of a hurricane's maximum sustained wind speed. In general, hurricanes with stronger winds are able to generate larger waves and stronger currents that result in more vertical mixing and cooling (Dare & McBride, 2011). Haakman et al. (2019) analyzed North Atlantic hurricane observations from 2002 through 2018 and found that while category-1 hurricanes caused the least amount of cooling, there was a difference of just ~0.1 ℃ in cooling beneath category-2 hurricanes and major hurricanes (category-3 through category-5), with category-2 hurricanes resulting in greater cooling. These finding are supported by Michaels et al. (2006) and Lloyd and Vecchi (2011). Lloyd and Vecchi (2011) surmise that this is due to the effect of the oceanic

cooling feedback on hurricane intensity. They argue that hurricanes can only generate so much oceanic cooling before they restrict their ability to intensify further, so the minimal differences in cooling between category-2 and major hurricanes is simply because category-2 hurricanes could not have developed into major hurricanes had they caused greater cooling beneath them. The authors also put forth another potential explanation in that wind speeds within a category-2 hurricane are strong enough to stir up waters of similar temperature as those stirred up by major hurricanes. Although major hurricanes may generate vertical mixing that penetrates deeper into the water column, the cooler waters brought to the surface are of comparable temperature to those brought to the surface by category-2 hurricanes, which could explain the insignificant difference in oceanic cooling between category-2 hurricanes and major hurricanes.

A second atmospheric factor shown to impact oceanic cooling is a hurricane's translation speed, which is the speed at which the system itself is moving. Hurricanes with slower translation speeds typically result in greater cooling, as slow-moving systems spend more time over fixed points in the ocean and therefore have greater time to generate vertical mixing and cooling (Bender et al., 1993). According to several studies, a hurricane's translation speed seems to have a greater impact on oceanic cooling than any other parameter (e.g., Haakman et al., 2019; Price, 1981). Haakman et al. (2019) examined the impact of two hurricane parameters and two oceanic parameters on oceanic cooling. The hurricanes parameters were the 10-minute maximum sustained wind speed and translation speed with the oceanic parameters being the barrier layer thickness and barrier layer potential energy. For each hurricane in their study, the authors determined the change in the sea surface temperature anomaly (ΔSSTA) within a 500 km radius of the hurricane center. They then developed three composite ΔSSTA fields for each parameter based on percentiles. For example, a composite ΔSSTA field was developed for the lowest one-

third, middle one-third, and highest one-third of maximum sustained wind speeds values to observe how oceanic cooling differed between the weakest, average, and most powerful hurricanes. The authors found that the greatest cooling occurred beneath the hurricanes with the highest maximum sustained wind speeds, the slowest translation speeds, and when the barrier layer thickness and barrier layer potential energy were lowest. The mean maximum ΔSSTA values from these composites were -1.94 ℃ (10-minute maximum sustained wind speed), -2.55 ℃ (translation speed), -2.14 ℃ (barrier layer thickness), and -2.29 ℃ (barrier layer potential energy). Low translation speeds caused the greatest amount of cooling, followed by low barrier layer potential energies and thin barrier layers. A hurricane's 10-minute maximum sustained wind speed proved to be the least important of the four parameters in regard to oceanic cooling.

An oceanic condition shown to affect oceanic cooling is the mixed layer depth (MLD). The MLD is the depth of uniformly mixed waters near the sea surface, and it can be defined by differences in temperature or density. The temperature defined MLD, or isothermal layer depth (*ITLD*), is often defined as the depth at which the ocean temperature is equal to the SST minus 0.5 ℃ (e.g., Price et al., 1986; Kelly & Qiu, 1995; Obata et al., 1996). The density defined MLD, or isopycnal layer depth (*IPLD*), has been defined as the depth at which potential density is equal to the potential density as the sea surface plus 0.125 kg m^{-3} (e.g., Miller, 1976; Spall, 1991). A relatively shallow MLD is beneficial for cooling because mixing does not have to occur as deep to stir up cooler waters from beneath the thermocline (Mao et al., 2000).

Greater cooling has also been shown to occur when the barrier layer thickness (*BLT*) is thin (Haakman et al., 2019). *BLT* is the vertical distance between the *ITLD* and *IPLD*. A larger *BLT* will mitigate the entrainment of cooler waters, thus limiting the overall cooling (Wang et al., 2011). This is because thicker barriers layers are often associated with smaller vertical

temperature gradients which mitigates the upward movement of cooler waters (Foltz & McPhaden, 2009). As mentioned above, in their ~20 year study on North Atlantic hurricanes, Haakman et al. (2019) found *BLT* to have a greater impact on oceanic cooling than hurricane strength as a function of its 10-minute maximum sustained wind speed.

An additional oceanic parameter that can impact cooling beneath hurricanes is the Brunt-Vaisala frequency (*N*). Developed by Vilho Vaisala and David Brunt, *N* is a metric that can be used to quantify the stability of a fluid in a statically stable environment. When a fluid parcel in such conditions becomes vertically displaced, a buoyancy force acts upon the parcel in an effort to return it to its initial position (Stull, 2011). Typically, the parcel will overshoot its initial position and the buoyancy force will change direction in an attempt to return the parcel once again to its original position. This process repeats itself, resulting in an oscillation that is measured in cycles per unit time. In oceanography, *N* can be defined as:

$$N = \sqrt{(-g\rho^{-1})(\Delta\rho z^{-1})}$$

where g is gravity, ρ is water density, and z is depth, with N typically expressed in cycles per second, or simply s^{-1}. *N* is thereby used to quantify the stratification of water with the column, with larger values denoting greater stratification.

1.3 The Relationship Between Tropical Cyclones, Cold Wakes, & Climate

A well-rounded understanding of hurricanes and cold wakes is critical as both play a pivotal role in Earth's climate system. Hurricanes gain energy from heat fluxes moving from warm ocean waters into the atmosphere. Thus, on a fundamental level, a hurricane's intensity is a function of the SST beneath the system (Emanuel, 1986). As cold wakes develop, a negative feedback loop is introduced as heat fluxes begin to decrease. The cold wake of Hurricane

Frances (2004) resulted in a 5 m s^{-1} decrease in the storm's maximum sustained wind speed (D'Asaro et al., 2007). Furthermore, Schade and Emanuel (1999) estimated that cold wakes have the potential to reduce hurricane intensity by up to 70%. It can take up to three weeks or more for SSTs to return to pre-storm levels following a hurricane (Mei & Pasquero, 2013). As such, cold wakes have the potential to impact both the hurricane that caused them, and any hurricane that passes in that region in the coming days, weeks, or months. Cold wakes have been shown to weaken future hurricanes (Cione & Uhlhorn, 2003), alter hurricane tracks (Bener et al., 2003), and shorten the hurricane season (Wendland, 1977).

One cold wake climate implication comes from the redistribution of heat within the water column. Though cold wakes are identified by the rising of cooler waters from beneath the thermocline, it is important to note the downward movement of warm surface waters that are transported below the mixed layer. Over time, the mixed layer returns to a state of equilibrium with surrounding waters through a combination of mixing and surface fluxes leading to an overall heating of the water column. Sriver and Huber (2007) surmise that this hurricane-induced heat redistribution contributes roughly 15% to the overall poleward transfer of heat. This additional heat transferred poleward thereby affects thermohaline circulation which is a critical and sensitive regulator of the broader climate system (Emanuel, 2001).

Further effects of hurricanes on climate occur with changes in atmospheric properties that result from upwelling. During the upwelling process, nutrient-rich waters are brought to the surface from depth. The excess of nutrients near the surface often results in phytoplankton blooms (Babin et al., 2004) that alter the air-sea flux of carbon dioxide (CO_2) (Bates et al., 1998). Another aspect of climate implications relates to the contribution of hurricanes to the efflux of CO_2 from the ocean. Flux measurements of CO_2 are important to understand because it is a

greenhouse gas (GHG) that has implications for the warming of Earth's climate. Due to its unique chemical structure, molecules of CO_2 absorb a considerable amount of long-wave radiation being emitted from the surface of the Earth, which they then redirect back towards Earth, resulting in greater warming (Mitchell, 1989). Since the onset of the industrial revolution in the late 18^{th} century, concentrations of CO_2 from anthropogenic sources have been on the rise. Since 1960, atmospheric concentrations of CO_2 have risen from ~320 ppm to ~420 (NOAA Climate, 2022). This is critical because increases in these GHGs such as CO_2 are likely to result in a continual warming of Earth's climate (Intercontinental Panel on Climate Change, 2018).

The world's ocean play a key role in the global carbon cycle as they act as a large sink for CO_2, absorbing an estimated ~30% of anthropogenic CO_2 since the beginning of the industrial revolution (Gruber et al, 2019). The determining factor for the direction and magnitude of air-sea CO_2 fluxes is the partial pressure of CO_2 (pCO_2) in both mediums (Sarmiento & Gruber, 2006). When the atmospheric pCO_2 is greater than the oceanic pCO_2, the CO_2 flux is directed from atmosphere into the ocean. Under these conditions, the ocean is undersaturated. If the oceanic pCO_2 is greater than the atmospheric pCO_2, the CO_2 moves from the ocean to the atmospheric. In these situations, the ocean is oversaturated.

Oceanic pCO_2 is highly dependent on temperature, with warmer ocean waters exhibiting larger pCO_2 values (Koch et al., 2009). Because higher ocean temperatures yield higher pCO_2 values, there is a higher likelihood of the waters being oversaturated when temperatures are higher. This is important because hurricanes are most likely to occur in the summer and autumn months when SSTs are highest as they are fueled by ocean-atmosphere heat fluxes. Thus, hurricanes have a high likelihood of translating over oversaturated ocean waters in which the flux of CO_2 is moving out of the ocean and into the atmosphere. Due to their anomalously high

wind speeds, hurricanes increase CO_2 fluxes due to enhanced air-sea interaction. Since hurricanes are more likely be to translating above oversaturated waters, they contribute greatly to the efflux of CO_2 from the ocean into the atmosphere. Although cooler waters exhibit lower partial pressures of CO_2, the decreases in oceanic partial pressure associated with hurricane-induced cooling are often not enough to reverse the direction of the flux, remaining an efflux from the ocean into the atmosphere (Bates et al., 1998). It is estimated that high wind speed events such as tropical storms and hurricanes are contributing between 0.042 and 0.509 Pg C y^{-1} from the ocean to the atmosphere (Bates et al., 1998).

1.4 Tropical Cyclone Forecasting

Accurate hurricane forecasting is important because it allows for adequate preparation and the mobilization of resources to assist with relief efforts following the storm. Hurricane forecasting can be broken down into two categories: track forecasting and intensity forecasting. Hurricane track forecasting is the prediction of where hurricanes are going to go, while intensity forecasting pertains to predicting changes in hurricane intensity. With advancing technologies and a better understanding of the mechanisms that control hurricanes, improvements have been seen in both of these divisions of hurricane forecasting. Figures 2 and 3 show the errors associated with National Hurricane Center (NHC) track forecasts and intensity forecasts from 1990 to 2021.

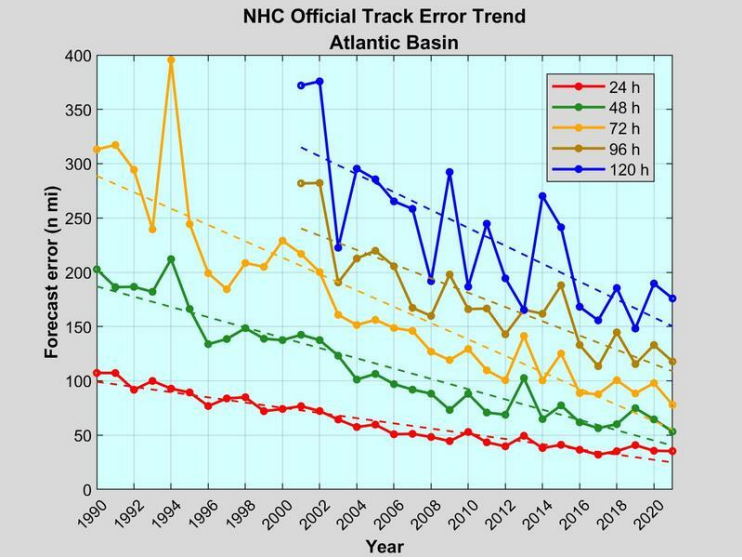

Figure 2:Error measurements associated with NHC hurricane track forecasts from 1990 to 2021. Error measurements are distances in nautical miles (n mi). Different colors pertain to forecasts for varying timescales. Figure from the NHC.

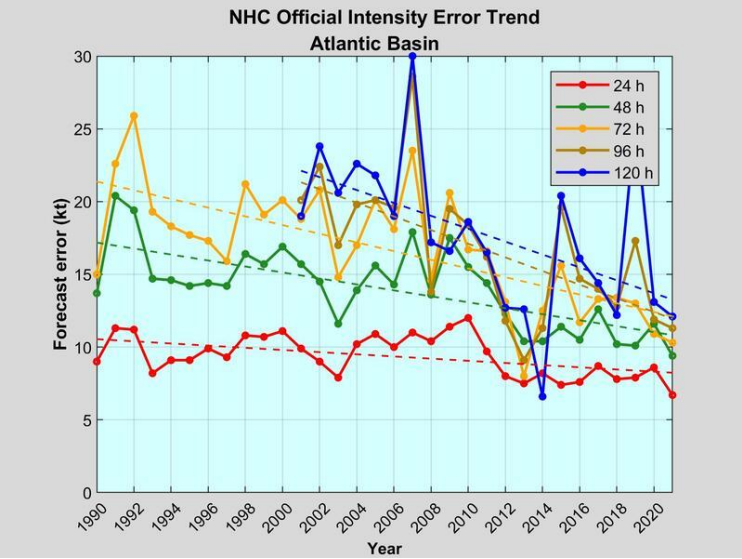

Figure 3: Error measurements associated with NHC hurricane intensity forecasts from 1990 to 2021. Error measurements are maximum sustained wind speeds in knots (kt). Different colors pertain to forecasts for varying timescales. Figure from the NHC.

One trend that can be identified from both these figures is the decrease in error associated with measurements closer out in time (e.g., lower errors in 24-hour forecasts vs. 120-hour forecasts). A second trend is the general decreases in both track forecast errors and intensity

forecast errors over the past three decades. However, it is well noted that while track forecast errors have seen significant improvement, intensity forecast errors have improved relatively little in comparison (Cangialosi & Franklin 2012; Demaria et al., 2014). Thus, a better understanding of mechanisms that influence hurricane intensity could potentially lead to improved intensity forecasts. Because cold wakes have direct impacts on hurricane intensity, further understanding of this oceanic cooling could ultimately lead to decreases in error measurements associated with hurricane intensity forecasts.

2. RESEARCH QUESTIONS & HYPOTHESES

1) Which individual hurricane and/or oceanic parameters have the greatest effect on hurricane-induced oceanic cooling?

Hypothesis 1: Hurricane parameters, principally storm strength and translation speed, will have the greatest impact on oceanic cooling and be able to explain more variance in oceanic cooling than oceanic parameters.

2) Which hurricane and/or oceanic parameters interact to result in greater oceanic cooling?

Hypothesis 2: The greatest cooling will occur when the hurricane is strong, has a slow translation speed, and the underlying ocean has a shallow isothermal layer.

3) The hurricane surface forcing is spatially nonuniform. How will the statistics change when using data that is closer to the hurricane center?

Hypothesis 3: Hurricane parameters will be more important to cold wake formation near the hurricane center and oceanic parameters will become more important further from the hurricane center.

3. DATA & METHODS

3.1 Tropical Cyclone Data

3.1.1 Background on Tropical Cyclone Data

The data used in this project comes from three sources. The first is Colorado State University's (CSU's) Extended Best Track (EBTRK) dataset, an expansive hurricane dataset that serves as an extension of the National Oceanic and Atmospheric Administration's (NOAA's) own hurricane dataset, HURDAT2. HURDAT2 contains records on North Atlantic hurricanes dating back to 1851, and is updated annually to include the most recent season's storms. To understand EBTRK it is important to have an understanding of its main source, HURDAT2. The HURDAT2 dataset is freely available from the NHC. The file is a large matrix with rows of time intervals and columns pertaining to different parameters or meta information. During the life of a storm, these data are recorded at six-hour intervals (00:00, 06:00, 12:00, and 18:00 Coordinated Universal Time). Each row in the dataset, referred to hereinafter as a tropical cyclone observation point (TCOP), thereby acts as a snapshot of a hurricane at a given time and location, with single values for latitude, longitude, maximum sustained wind speed, etc.

Figure 4 is an example of the layout of HURDAT2 for Hurricane Katrina (2005). To mark the beginning of a new storm, there is a row containing the storm's ID, name, and the number of rows to follow that pertain to that storm. For rows containing data, the parameters recorded are as follows: date; time; record identifier; storm status; latitude; longitude; maximum sustained wind speed; minimum pressure; radius of 34 kt sustained winds in the northeast, southeast, southwest, and northwest quadrants; radius of 50 kt sustained winds in the northeast, southeast, southwest, and northwest quadrants; and radius of 64 kt sustained winds in the

northeast, southeast, southwest, and northwest quadrants. In total, there are 20 parameters recorded for each TCOP. Missing data values for any of these columns are entered as "-999."

```
AL122005,            KATRINA,     34,
20050823, 1800,  , TD, 23.1N,  75.1W,  30, 1008,    0,    0,    0,    0,    0,    0,    0,    0,    0,    0,    0,    0,
20050824, 0000,  , TD, 23.4N,  75.7W,  30, 1007,    0,    0,    0,    0,    0,    0,    0,    0,    0,    0,    0,    0,
20050824, 0600,  , TD, 23.8N,  76.2W,  30, 1007,    0,    0,    0,    0,    0,    0,    0,    0,    0,    0,    0,    0,
20050824, 1200,  , TS, 24.5N,  76.5W,  35, 1006,   60,   60,    0,    0,    0,    0,    0,    0,    0,    0,    0,    0,
20050824, 1800,  , TS, 25.4N,  76.9W,  40, 1003,   60,   60,    0,    0,    0,    0,    0,    0,    0,    0,    0,    0,
20050825, 0000,  , TS, 26.0N,  77.7W,  45, 1000,   60,   60,    0,    0,    0,    0,    0,    0,    0,    0,    0,    0,
20050825, 0600,  , TS, 26.1N,  78.4W,  50,  997,   60,   60,    0,    0,   15,    0,    0,    0,    0,    0,    0,    0,
20050825, 1200,  , TS, 26.2N,  79.0W,  55,  994,   60,   60,   30,   50,   20,   20,    0,    0,    0,    0,    0,    0,
20050825, 1800,  , TS, 26.2N,  79.6W,  60,  988,   70,   70,   50,   60,   25,   25,   20,   20,    0,    0,    0,    0,
20050825, 2230, L, HU, 26.0N,  80.1W,  70,  984, -999, -999, -999, -999, -999, -999, -999, -999, -999, -999, -999, -999,
```

Figure 4: An example of the HURDAT2 data file from the NHC showing the first ten TCOPs of Hurricane Katrina (2005).

3.1.2 Explanation of Tropical Cyclone Parameters

Hurricane intensity within HURDAT2 is measured as a function of the one-minute maximum sustained wind speed at an altitude of 10 m. There are several methods in which these measurements are obtained, one is the Dvorak Technique (Figure 5) which utilizes satellite imagery to allow for experts to gauge the strength of a hurricane based on factors such as cloud band patterns, size of the central dense overcast (CDO), and more (Dvorak, 1975).

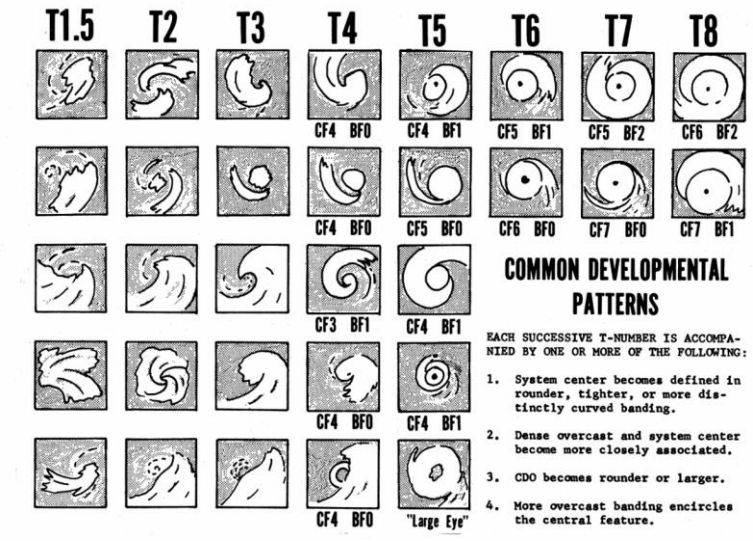

Figure 5: A graphical representation of various hurricane structures and how they would be classified using the Dvorak Technique, along with a short list of frequent development patterns. Modified from Figure 2 in Dvorak (1975).

Additional measurements of wind speeds via satellite are obtained from satellites equipped with a scatterometer. Scatterometers are active sensors that emit microwaves and record the backscatter which varies with the roughness of the sea surface. In general, wind speed and sea surface roughness are highly correlated with higher wind speeds being associated with rougher sea surfaces. Thus, scatterometers are useful instruments for estimating 10 m wind speeds (Chan & Chan, 2012). An advantage to determining wind speeds using scatterometers is that by using microwaves, cloud cover can be easily penetrated. This allows for relatively unobstructed observations (Tomiyasu, 1974).

A third method to obtain wind speed values comes from aircraft reconnaissance missions and dropsondes. As hurricanes approach land, specially equipped aircraft operated by the United States military or government agency such as NOAA are flown into the storm to gather real time data. These aircraft often carry dropsondes which are released from the aircraft and record wind speed, wind direction, temperature, pressure, and humidity as they descend to the sea surface (Halverson et al., 2006). Wind speed data from these missions can then be adjusted down to 10 m (Franklin et al., 2003).

Six of the ten parameters of interest for this study are hurricane parameters. This includes the maximum sustained wind speed (V_{max}), minimum sea level pressure (P_{min}), translation speed (U_h), radius of maximum winds (RMW), time available for vertical mixing (LU_h^{-1}), and tropical cyclone latitude (Lat_{TC}). V_{max}, a function of hurricane strength, is included in this study because it has been previously correlated with oceanic cooling (Haakman et al., 2019; Price, 1981). A second metric of hurricane strength, P_{min}, has not been explicitly studied in relation to cold wakes to the degree of V_{max}. Since it is available within the EBTRK, P_{min} has been included in this study to allow for a side-by-side comparison of both hurricane strength metrics on oceanic

cooling. As with V_{max}, U_h has been included because it has also been shown to have an impact on oceanic cooling beneath hurricanes, even more so than V_{max} (Haakman et al., 2019; Price, 1981). Also included in the study is *RMW*, a metric of hurricane size. This parameter has been included with the mindset that hurricane with a higher *RMW* (greater spatial coverage) will spend more time mixing the upper ocean, potentially resulting in greater cooling. Taking this a step further, LU_h^{-1} is a temporal metric of vertical mixing that takes both hurricane size and translation speed into consideration (Shay et al., 2000).

V_{max}, P_{min}, *RMW*, and Lat_{TC} are all provided in the EBTRK dataset, with U_h and LU_h^{-1} being calculated using information from EBTRK. Hurricane data in EBTRK is recorded in six-hour intervals. U_h is calculated by taking the latitude and longitude of a TCOP, the latitude and longitude of the previous TCOP, finding the great circle distance between those two points, and dividing the distance by six hours (Kossin, 2018). This yields a translation speed in km hr^{-1}. Given two successive TCOPs (*a* and *b*), the great circle equation used to solve for the U_h of TCOP *b* is:

$$U_h = r_{Earth}*acos((cos(90 - Lat_a)*cos(90 - Lat_b)) + (sin(90 - Lat_a)*sin(90 - Lat_b)*cos(Lon_a - Lon_b))) / 6$$

where r_{Earth} is the radius of Earth (6,371 km) and with all latitude and longitude values being converted from degrees to radians. Multiplying this by 1,000 and dividing by 21,600 converts U_h from km hr^{-1} to m s^{-1}. The second calculated metric, time available for vertical mixing, is given by the equation:

$$LU_h^{-1} = (2*RMW)/U_h$$

(Shay et al., 2000) which yields the time available for vertical mixing value in seconds. Dividing this by 3,600 gives the time available for vertical mixing in hours. Large, slow-moving hurricanes will have longer LU_h^{-1} meaning they have more time to generate vertical mixing.

3.1.3 Uncertainties of Tropical Cyclone Data

HURDAT2 contains roughly 170 years of data on hurricane activity in the North Atlantic. Because of this long record, it must be noted that data further back in time will have larger uncertainties and errors. These uncertainties are due to a variety of factors, but mainly the differences in technologies available throughout the record. The development and implementation of satellite remote sensing in the 1970s greatly improved the accuracy of hurricane measurement. Experts at the NHC estimate errors in wind speed measurements of minor hurricanes (category-1 and -2 on the Saffir-Simpson Hurricane Wind Scale (SSHWS)) to be 12 kt when only satellite data is used and 8 kt when a combination of satellite and aircraft reconnaissance data are used (Landsea & Franklin, 2007). These values increase to 14 kt and 11 kt respectively for major hurricanes (category-3, -4, and -5 on the SSHWS). Errors in minimum central pressure values of minor hurricanes are 8 mbar, increasing to 10 mbar for major hurricanes. The data for this project range from 2003 through 2019 so larger errors associated with older measurements (pre-satellite) are not a concern.

3.1.4 Summary of Tropical Cyclone Data

The EBTRK dataset is a summation of HURDAT2, with the addition of four parameters: radius of maximum wind speed, eye diameter (if applicable), pressure of the outer closed isobar, and radius of the outer closed isobar, This dataset is freely available from CSU's Regional and Mesoscale Meteorology Branch. Its structure is the same as HURDAT2, with additional columns for the new parameters. *RMW* first became available in EBTRK for hurricanes in 2003 which is

why the project begins with data from that year. Data for this project go through 2019 because this was the final year in which hurricane data was available within HURDAT2 and EBTRK at the beginning of data collection in spring 2021.

3.2 Oceanic Data from Argo Floats

3.2.1 Background on Argo Floats

The second source of data for this project is Argo floats, for the purpose of understanding upper-ocean structure prior to the arrival of hurricanes. The Argo program consists of an array of floats that are scattered around the world's oceans. It is an international collaboration headed by the Argo Steering Team. The program began in 2000, and as of September 2022 there are 3,885 operational floats collectively maintained by 23 countries (NOAA Atlantic Oceanography Meteorological Laboratory (AOML) Physical Oceanography Division (PhOD)). Figure 6 shows the global spatial distribution of these floats, color coded by the individual country responsible for its deployment and upkeep.

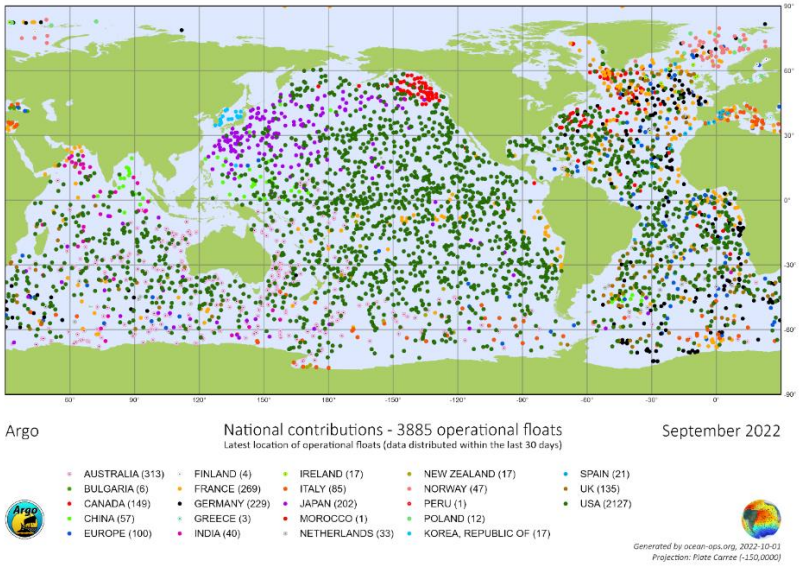

Figure 6: The global spatial distribution of all 3,885 operational Argo floats as of September 2022. Floats are represented by dots that are color coded based on the country responsible for its operation. Image generated by ocean-ops.org.

3.2.2 Explanation of Argo Float Data Collection Process

The majority of Argo floats operate as conductivity, temperature, and depth (CTD) profilers. Other types of Argo floats include biogeochemical (BGC) floats. In addition to gathering CTD data, BGC floats are equipped with additional sensors to record parameters such as oxygen concentration, nitrogen concentration, pH, chlorophyll-a, suspended particles, and downwelling irradiance (Biogeochemical Argo, 2021). However, only data from standard CTD measurements are used in this study.

Argo floats are usually deployed into the ocean via ship, but can also be deployed from aircraft. Once deployed, the float descends to a depth of 1,000 m at a rate of around 10 cm s^{-1}. Upon reaching this depth, the float maintains depth and travels along with ocean currents for roughly nine days. At this point, the float further descends to 2,000 m before beginning a slow ascent back to the sea surface. During its ascent, the float records data with onboard sensors. Conductivity measurements are used to derive salinity in practical salinity units (PSU), and pressure measurements are used to derive depth. Once a float reaches the surface, it is located via a global positioning system, at which points it transfers the data recorded during its ascent to a data acquisition center (DAC). After the transfer process is complete, the floats descends back to 1,000 m to begin this process that it will repeat for the remainder of its life (Jayne et al., 2017).

The vertical movement of each float is controlled by an internal oil pumping mechanism (NOAA AOML PhOD). Each float is equipped with a compartment that stores oil. While this oil is located in the internal compartment, the float will descend as it is less buoyant than the surrounding waters. When the float reaches the depth where it is ready to begin its ascent, oil is pumped into an external bladder, increasing the float's buoyancy and allowing it to rise to the sea surface.

3.2.3 Quality Control Process of Argo Float Data

Once data from a float arrives at a DAC, it undergoes a strict quality control (QC) process consisting of 18 tests listed in Table 1. The primary goal of these tests is to ensure no bad data becomes available for download (Wong et al., 2013). Sensors and floats that return profiles with data that do not pass all these tests are flagged in case the float and/or sensor are no longer viable. The first 17 tests are automated and completed by computers at the DAC. The 18th and final test is a visual QC test performed by an expert. Since this test is more time consuming and the automated tests are more than likely to catch any errors, the visual QC test is performed as assurance once the data have already been made available. Once data from a profile has passed these tests, it is sent onward to both of Argo's global data assembly centers (GDACs) located in Monterey, California and Brest, France. At this stage, data become available for download to the public. Ideally, data will make it through each of the first 17 QC tests and become available for download within 24 hours from the transmission from the float. CTD data from Argo float profiles is highly accurate. The error for temperature measurements is ±0.002 °C, and the pressure measurements having an error of ±2.4 dbar (University of California, San Diego). The error associated with salinity values from conductivity measurements is ±0.01 PSU.

Table 1: A list of the 18 QC tests completed on Argo data. The list is in chronological order of test completion.

Order	Test Name
1	Deepest Pressure Test
2	Platform Identification Test
3	Impossible Date Test
4	Impossible Location Test
5	Position on Land Test
6	Impossible Speed Test
7	Global Range Test
8	Regional Range Test
9	Pressure Increasing Test
10	Spike Test
11	Gradient Test
12	Digit Rollover Test
13	Stuck Value Test
14	Density Inversion Test
15	Grey List Test
16	Gross Salinity or Temperature Sensor Drift Test
17	Frozen Profile Test
18	Visual QC Test

3.2.4 Calculation of Oceanic Parameters from Argo Floats

There are no designated depths at which data is collected by an Argo float. As such, measurements of temperature and conductivity are taken at arbitrary depths about every two meters. For example, data within a profile may be collected at 10.26 m, 12.94 m, 14.68 m, and so on. To adjust for this unevenness, an interpolation was performed on each Argo float profile so that temperature and conductivity are at integer depths. Figure 7 shows an example Argo float profile with the interpolated depths and temperatures laid over the raw values. Due to the nature of the hardware, Argo floats are unable to record data right at the air-sea boundary. For the majority of profiles, the shallowest measurement ranges anywhere from about one to eight meters. After the interpolation of each profile was complete, the shallowest 1 m depth interval

was determined and any missing values between that depth and the surface were added on using values from that shallowest interval.

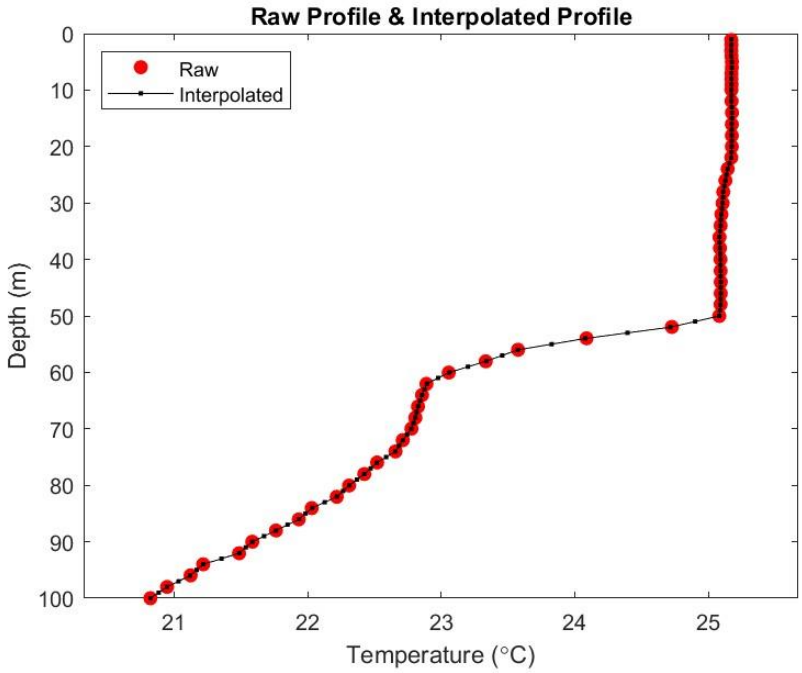

Figure 7: An example Argo float profile with red circles showing the raw temperature/depth measurements and the black line with black dots showing the interpolated temperature/depth values (every one meter).

Four of the ten parameters of interest are oceanic parameters calculated using data from Argo float profiles. These four parameters are the *ITLD*, *IPLD*, *BLT*, and *N*. The *ITLD* is often defined as the depth at which the ocean temperature is 0.5 °C lower than the *SST* (e.g., Price et al., 1986; Kelly & Qiu, 1995; Obata et al., 1996). In calculating this parameter, the first step was to determine the temperature of the *ITLD* which was done with the equation:

$$ITLD_{temp} = SST - 0.5$$

where $ITLD_{temp}$ is the temperature of the *ITLD*. The index of the $ITLD_{temp}$ value in the temperature profile was then used to find the corresponding depth to determine the *ITLD*. The *IPLD* is defined as the depth at which the ocean potential density is equal to the sea surface

potential density plus 0.03 kg m^{-3} (Thomson & Fine, 2003). The potential density at the *IPLD* was calculated with the equation:

$$IPLD_{pdens} = SS_{pdens} + 0.03$$

where $IPLD_{pdens}$ is the potential density at the *IPLD* and SS_{pdens} is the potential density at the sea surface. The index of the $IPLD_{pdens}$ was then used to locate the associated depth to determine the *IPLD*. The *BLT* is equal to the vertical distance between the *ITLD* and *IPLD*, and was calculated with the equation:

$$BLT = ITLD - IPLD$$

Figure 8 shows the upper 100 m of an Argo float profile with markings for the *ITLD, IPLD,* and *BLT*.

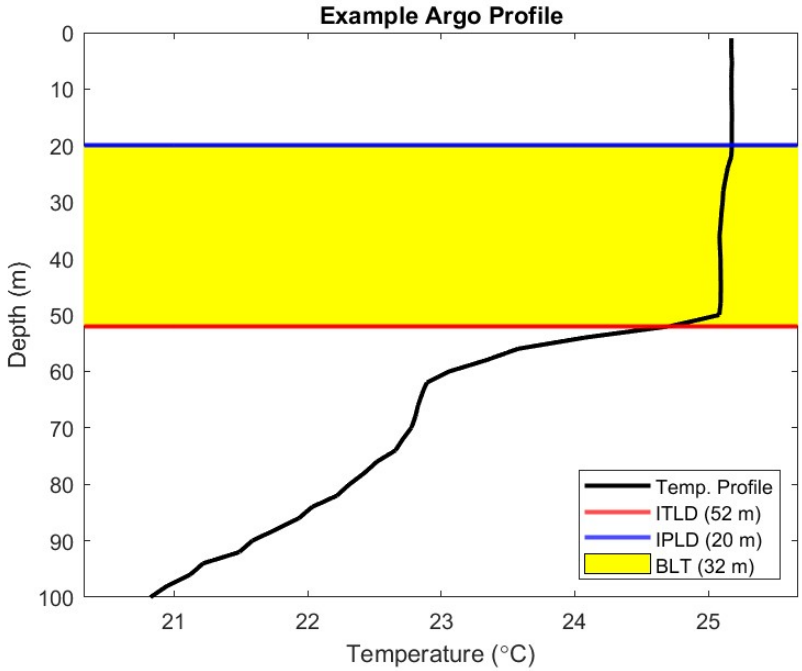

Figure 8: An example of the temperature profile of an Argo float from the surface to 100 m depth. The black line represents temperature, the red line indicates the ITLD, the blue line indicates the IPLD, and the shaded yellow section shows the barrier layer.

3.3 Oceanic Data from Satellites

3.3.1 Overview of Satellites

The development of satellite remote sensing in the early 1970s drastically altered the way scientists could observe the Earth, as satellites were able to record data over large areas in relatively short periods of time. While earlier satellites like Landsat-1 were focused on obtaining measurements over land, the National Aeronautics and Space Administration's (NASA's) Seasat became the first oceanographic-focused satellite when it was launched into orbit in 1978 (Born et al., 1979). Though Seasat was only operational for three months, it set a precedent for the capabilities of oceanographic satellites to come.

Satellites can carry a wide array of sensors to accomplish a multitude of tasks. Each of these sensors falls into one of two fundamental categories: active or passive. The difference between active and passive sensors is the source of the signal they receive. Active sensors emit their own signal and make observations based on the reception of that signal as it returns to the satellite. Passive sensors take measurements based on signals emitted or reflected by the Earth itself. The only satellite parameter used in this project is SST, used to determine oceanic cooling. SSTs are measured by a radiometer, a passive sensor which measures electromagnetic radiation emitted from the sea surface. From these measurements, SST is derived through a series of algorithms (Maurer, 2002). Notable radiometers include the Advance Very High Resolution Radiometer (AVHRR), the Moderate Resolution Imaging Spectroradiometer (MODIS), and the Visible Infrared Imaging Radiometer Suite.

3.3.2 NASA JPL GHRSST Level 4 SST Analysis Product

The third and final source of data for this project will be NASA's Jet Propulsion Laboratory's (JPL's) Group for High Resolution Sea Surface Temperature (GHRSST) Level 4

SST Analysis product. Data available from this product are nighttime skin measurements from an array of sensors including MODIS onboard Terra and AVHRR-3 onboard NOAA-19. The data recorded by these sensors is first gridded, then an optimal interpolation is performed to fill in any gaps (GHRSST Science Team, 2010). The dataset features global coverage of Earth's surface with data available from 1 June 2002 onward (JPL Multi-scale Ultra-high Resolution (MUR) MEaSUREs Project, 2015). The spatial resolution of the data provided is 0.1 ° longitude by 0.1 ° latitude (111 km by 111 km), with a temporal resolution of one day. As with the last two sources, this data is free to access and can be obtained from NASA's JPL's Physical Oceanography Distributed Active Archive Center.

3.4 Methods

3.4.1 Data Collection

The first step was to identify TCOPs in EBTRK where the maximum sustained wind speed was at least category-1 status (≥64 kt). This was necessary because EBTRK and HURDAT2 both contain data on tropical storms and tropical depressions in addition to hurricanes. Once these TCOPs had been isolated, if possible, they were matched with an Argo float profile that was used to provide the upper ocean conditions prior to the arrival of the hurricane. There were two criteria for an Argo float profile to be matched with a TCOP. The first being that the location of the Argo float must be within a distance of four times the radius of maximum winds (4xRMW) from a given TCOP. The second condition was that the Argo float recorded that profile no earlier than ten days before the arrival of the hurricane. These criteria ensured that the profiles used were representative of the oceanic conditions at the location of and leading up to the arrival of the hurricane. If multiple Argo float profiles matched with a single TCOP, only the float closest to the hurricane's *RMW* was retained as waters closest to the *RMW*

are likely more influenced by the system. If an Argo float profile matched with multiple TCOPs, only the match with the shortest distance between the float and TCOP was kept. TCOPs that did not match with any Argo float profiles were discarded.

The final step in data collection was to gather satellites SSTs for the time and location of each Argo float profile that had been retained. SSTs were gathered for the seven days leading up to, the day of, and the seven days following each TCOP. These SSTs were used to derive surface cooling (*ΔSST*) at the location of the Argo profile. Following Zhang et al. (2019), *ΔSST* is defined as the post-storm SST minus the pre-storm SST, with the post-storm SST being the average SST from days -7 through -2, and the post-storm SST being the SST for day +2. For reference, day 0 is the day associated with the TCOP.

SST and *ΔSST* were defined using satellite data instead of data from Argo float profiles for several reasons. For one, it allows for consistency among SST measurements across all of the data points. As mentioned above, the shallowest depth value in the Argo floats ranged from one to eight meters. If SSTs were to be derived from the Argo float profiles, then some SST measurements would be extrapolations from 8 m depth. Satellite data ensures an accurate, skin-level temperature measurement of the sea surface. Additionally, if Argo SSTs were used to define pre-storm SSTs, then *ΔSST* values would be the difference of two different products: Argo float profiles (pre-storm SST) and satellites (post-storm SST). Since satellite SSTs are necessary to determine the post-storm SST, then it is best practice to also obtain the pre-storm SST using the same product so uncertainties associated with different products do not need to be considered.

A list of all the parameters gathered or calculated for this project is shown in Table 2. After data collection was complete, a dataset matrix was constructed to house all the data. Each

row in the matrix represented an individual event, with single values for each of the parameters from Table 2. Once the dataset had been constructed, linear regression, principal component analysis (PCA), analysis of variance (ANOVA), and multilinear regression (MLR) were performed to look for relationships between the parameters and *ΔSST*. To address *Hypothesis 3* regarding how the statistics would change with different distance metrics, three other datasets were constructed. The original dataset contained data within 4x the RMW (all data). The other three only contained the data within 3x, 2x, and 1xRMW.

Table 2: A list of the parameters gathered or calculated from the three sources of data, along with respective abbreviations and units.

Parameter	Abbreviation	Units
Maximum Sustained Wind Speed	V_{max}	kt
Minimum Sea Level Pressure	P_{min}	mbar
Translation Speed	U_h	m s^{-1}
Radius of Maximum Winds	*RMW*	km
Time Available for Vertical Mixing	LU_h^{-1}	hr
Tropical Cyclone Latitude	Lat_{TC}	°N
Isothermal Layer Depth	*ITLD*	m
Isopycnal Layer Depth	*IPLD*	m
Barrier Layer Thickness	*BLT*	m
Brunt-Vaisala Frequency	*N*	s^{-1}
Cooling	*ΔSST*	°C

3.4.2 Statistical Analysis

The preliminary method of statistical analysis was linear regression. For each TCOP, the *ΔSST* of that event was run against the remainder of the parameters listed in Table 2. These analyses provided the significance of the relationship between each parameters and *ΔSST*, as well as the amount of variance in *ΔSST* that could be attributed to each individual parameter. The

second method of statistical analysis was PCA, the purpose of which being to reduce the dimensionality of the datasets in an effort to simplify interpretation and identify parameters that work in tandem to contribute to oceanic cooling. When a PCA is performed, a series of modes are created, with the number of modes being equal to the number parameters being analyzed. Each mode is associated with an eigenvalue, as well as an eigenvector. An eigenvalue represents the amount of variance explained by a given mode. The first mode will have the largest eigenvalue and subsequent modes will have a lower eigenvalues. Each mode is also associated with an eigenvector, with each value in that vector acting as a loading for one of the parameters in the PCA. Parameter values from the original dataset can then be multiplied by their respective loading values for a given mode to yield a PCA score for said mode. A loading that is further from zero will have a greater impact on its respective PCA score. In addition to analyzing loading values for parameters within each mode, select mode scores form the PCA were scattered and color coded by hurricane category to identify any possible trends between hurricane category and mode scores. The spatial distributions of mode scores within the basin were also examined to identify potential relationships. Furthermore, ANOVA tests were performed to identify differences in mode scores between different months. The spatial distribution of different mode scores was also plotted to identify spatial trends of these scores within the North Atlantic basin.

The third method of statistical analysis on ΔSST was ANOVA. The benefit of an ANOVA test is that it allows for the testing of statistical differences among categorical data as opposed to quantitative data. In this project two ANOVA tests were run on ΔSST, one binning by month and the other binning by hurricane category. The purpose of these tests being to identify whether more cooling occurred during different times in the hurricane season, or between

hurricanes of different categories. The fourth and final method of statistical analysis came through the development of a MLR model, with ΔSST acting as the outcome variable. Chosen predictor variables were those that had the greatest influence on ΔSST based on the linear regressions and PCA. The goal was to develop a MLR model that could explain the most variance in ΔSST, using the fewest number of predictor parameters.

3.5 Examination of Data

There are 275 TCOPs spanning 67 hurricanes in the North Atlantic basin between 2003 and 2019 that are used in this study. The tracks of these hurricanes are presented in Figure 9. Each of these 67 hurricanes have at least one TCOP that was matched with an Argo float profile providing the pre-hurricane oceanic conditions. An example of the completed matching process for Hurricane Igor (2010) can be seen in Figure 10. The spatial distribution of all 275 TCOPs and their associated Argo float profiles is shown in Figure 11. The average distance between TCOPs and their associated Argo floats is 111.6 km with a standard deviation of 88.5 km. The median distance between TCOPs and their floats is 90.4 km. The shortest distance between a TCOP and Argo float is 12.5 km, which occurred with Hurricane Jeanne (2004). The greatest distance is 716.4 km, associated with Hurricane Michael (2018).

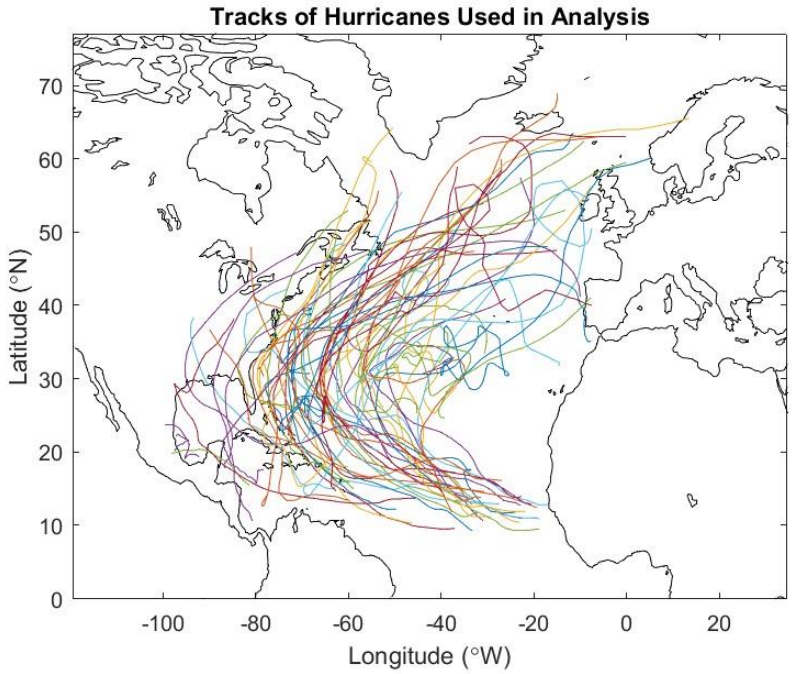

Figure 9: Tracks of the 67 hurricanes in the North Atlantic basin that have at least one TCOP used in analysis.

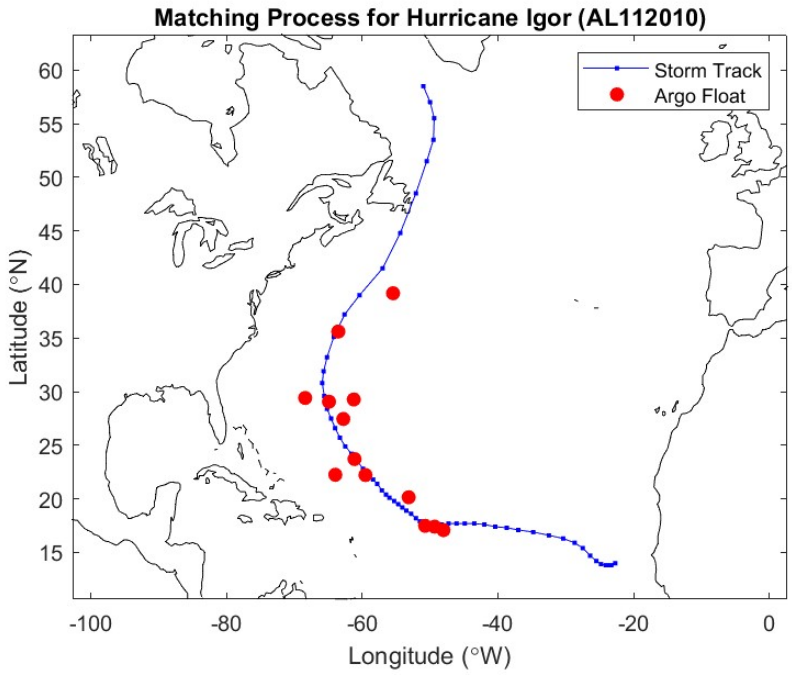

Figure 10:The track of Hurricane Igor (2010) along with the 13 Argo float profiles that matched with particular TCOPs. The blue line represents the track with blue squares indicating TCOPs. Argo float profiles are represented by red dots.

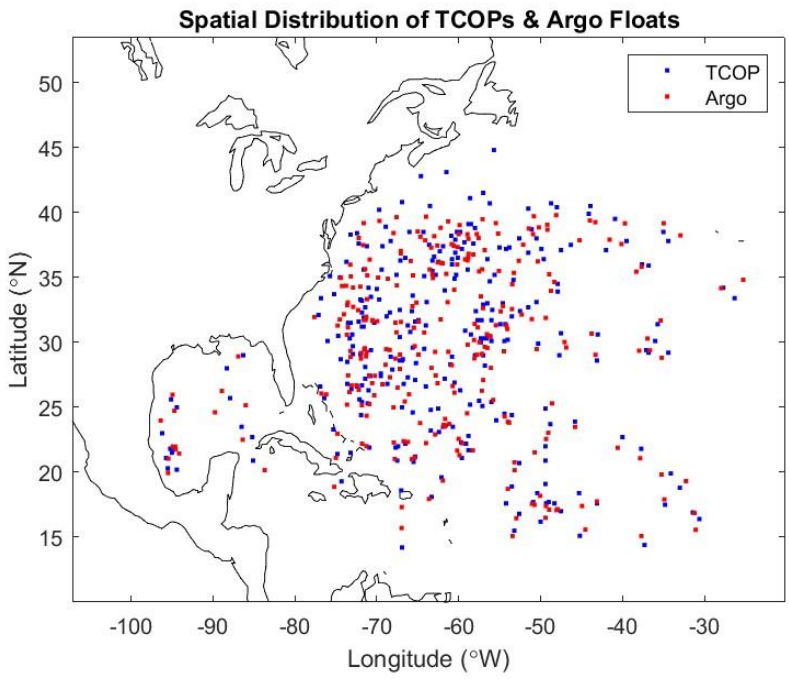

Figure 11: The spatial distribution of TCOPs and their associated Argo float profiles. Blue squares indicate TCOPs and red squares indicate Argo float profiles.

The data points not only span a wide geographic area, but also a large timeframe. A histogram of the data points by year and month can be seen in Figures 12a and 12b respectively. There is at least one data points per year from 2003 through 2019. The average number of data points per year is 16.2 with a standard deviation of 9.9. The majority of data points are present in the years 2010 (37) and 2017 (36). Conversely, the years with the least data points are 2013 (1) and 2007 (2). The three months with the most data points are September, October, and August with 138, 67, and 51 data points each. This is followed by July with 9, November with 6, December with 3, and June with 1. The data also cover the full range of hurricane categories on the SSHWS, though the distribution is not even. A histogram of hurricane category is shown in Figure 13. Most of the data comes from minor hurricanes, with 158 data points belonging to category-1 hurricanes and 58 to category-2 hurricanes. The remaining 21.5% of data come from

major hurricanes with category-3, -4, and -5 hurricanes having 39, 19, and 1 data points respectively.

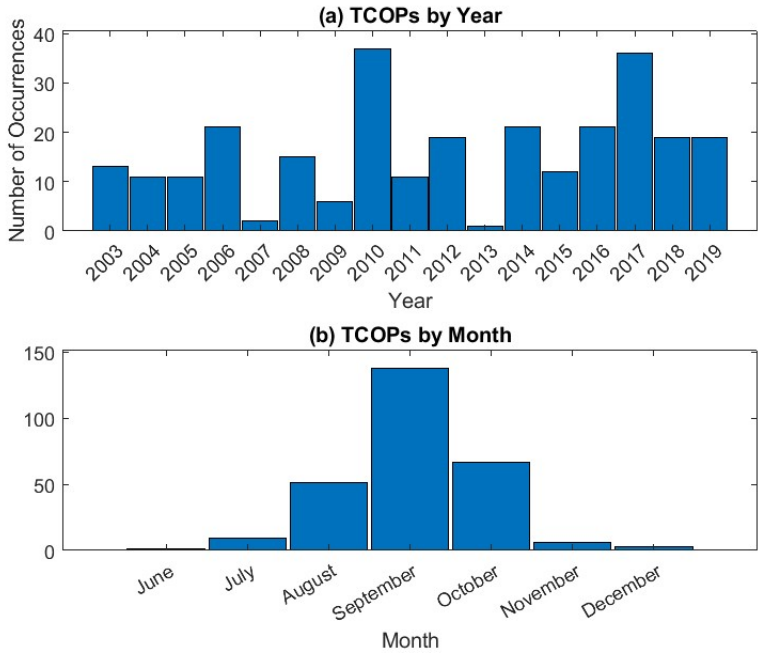

Figure 12: A histogram of the number of data points by (a) year and (b) month.

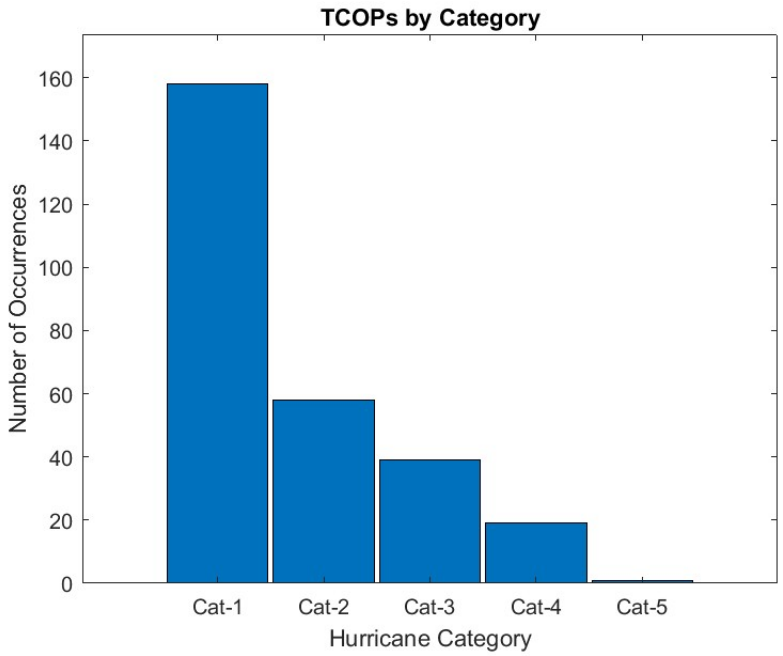

Figure 13: A histogram of the number of data points by hurricane category on the SSHWS.

As mentioned prior, satellite SSTs were gathered at each data point for the seven days leading up to, the day of, and the seven days following each hurricane. Figure 14a shows a timeseries of the change in SST from day -7 for each data point to help visualize the onset and development of each cold wake. The average ΔSST of all the cold wakes was 1.1 °C with a standard deviation of 0.9 °C. The greatest cooling was 4.8 °C underneath Hurricane Danielle (2010) when it was a strong category-2 hurricane (V_{max} = 95 kt). The least amount of cooling was actually 1.1 °C increase in SST after the passing of Hurricane Gordon (2006) which was also a category-2 hurricane at the time (V_{max} = 85 kt). Figure 14b shows average SST change for the four datasets (4x, 3x, 2x, and 1xRMW), having 275, 205, 137, and 38 data points respectively.

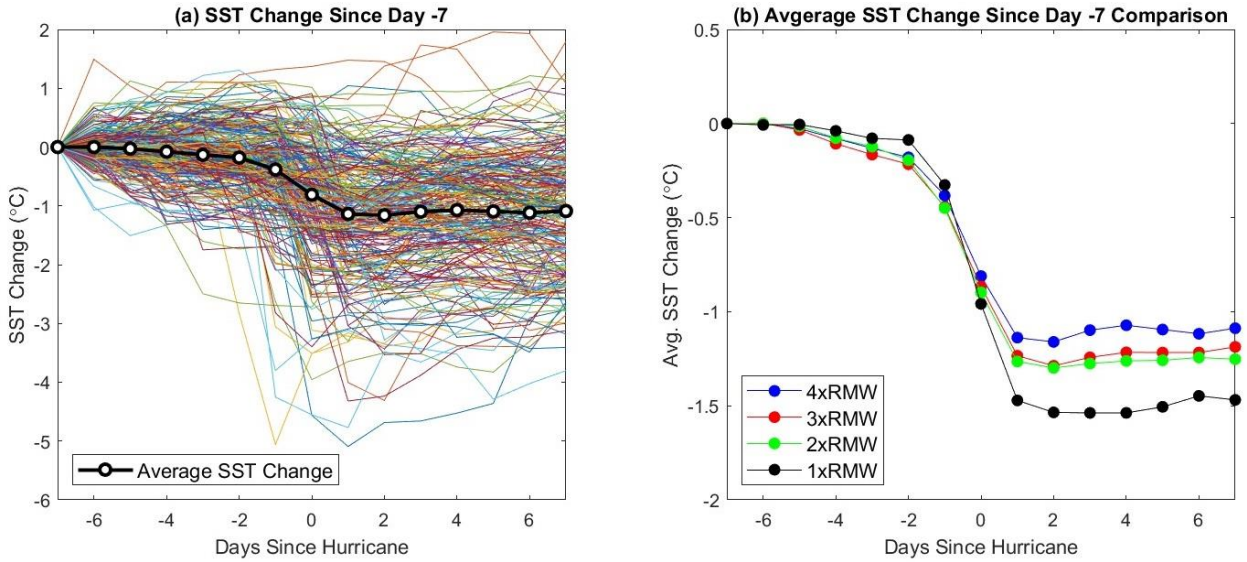

Figure 14: (a) SST change and average SST change from day -7 for day -7 through +7 for all data. Different colored lines indicate the each of the 275 data points. The black line with white dots represents the average SST change of all 275 data points. (b) Comparison of the average SST change from day -7 for data within different distance ranges from the hurricane center. The blue line (4xRMW) is equal to the black line with white dots in 14a.

4. RESULTS

4.1 Linear Regression

Table 3 shows the p-values and r^2 values associated with linear regressions of *ΔSST* against each of the ten hurricane and oceanic parameters listed in Table 2. The 4x, 3x, and 2xRMW datasets each have the same seven parameters that yield statistically significant relationships with *ΔSST* (p-value < 0.05). These are V_{max}, P_{min}, U_h, LU_h^{-1}, *ITLD*, *IPLD*, and *N*. The three remaining parameters (*RMW*, Lat_{TC}, and *BLT*) do not have statistically significant relationships with *ΔSST*. In the 1xRMW dataset, just three parameters have statistically significant relationships with *ΔSST*. These three parameters are P_{min}, U_h, and LU_h^{-1}. Of the three datasets in which the same seven parameters have statistically significantly relationships with *ΔSST* (4x, 3x, 2xRMW), parameters in the 2xRMW dataset can explain the most variance in *ΔSST*. Because of this, the remaining results from statistical analyses are focused on this dataset. Comparison of how these results differ among the other datasets is touched on in the discussion.

Table 3: P-values and r^2 values from linear regressions on data within 4x, 3x, 2x, and 1xRMW. The numbers in parentheses indicate the number of datapoints in each dataset. The total r^2 values do not include U_h or RMW because those are considered in LU_h^{-1}.

Parameter	4xRMW (275)		3xRMW (205)		2xRMW (137)		1xRMW (38)	
	p-value	r^2	p-value	r^2	p-value	r^2	p-value	r^2
V_{max}	0.01	0.025	0.03	0.023	0.03	0.033	0.1	0.075
P_{min}	<< 0.01	0.062	<< 0.01	0.065	<< 0.01	0.093	0.01	0.16
U_h	<< 0.01	0.103	<< 0.01	0.099	<< 0.01	0.158	<< 0.01	0.263
RMW	0.74	<< 0.001	0.86	<< 0.001	0.99	<< 0.001	0.73	0.003
LU_h^{-1}	<< 0.01	0.101	<< 0.01	0.123	<< 0.01	0.173	<< 0.01	0.271
Lat_{TC}	0.5	0.002	0.64	0.001	0.4	0.005	0.29	0.031
ITLD	<< 0.01	0.053	<< 0.01	0.045	<< 0.01	0.058	0.35	0.024
IPLD	<< 0.01	0.023	0.03	0.023	0.04	0.03	0.11	0.07
BLT	0.43	0.002	0.69	<< 0.001	0.74	<< 0.001	0.17	0.053
N	<< 0.01	0.037	0.01	0.036	0.01	0.054	0.14	0.06
Total		**0.305**		**0.316**		**0.446**		**0.744**

Figure 15 shows graphs of the linear regressions of *ΔSST* with the four hurricane parameters that have statistically significant relationships with *ΔSST*. Each of these regressions come from data in the 2xRMW dataset. The parameter that is able to explain the most variation in *ΔSST* is LU_h^{-1} with an r^2 value of 0.173. The next two parameters that explain the most variance in *ΔSST* are U_h (which is considered in LU_h^{-1}) and P_{min} with r^2 values of 0.158 and 0.093 respectively. The other hurricane strength metric, V_{max}, has an r^2 value of 0.033 for comparison. Figure 16 depicts the linear regression graphs of all four oceanic parameters with *ΔSST*. Three of the four oceanic parameters considered have statistically significant relationships with *ΔSST*. This includes *ITLD*, *N*, and *IPLD* with r^2 values of 0.058, 0.054, and 0.03 respectively. *BLT* yielded an insignificant p-value of 0.74, corresponding with an r^2 value of << 0.001.

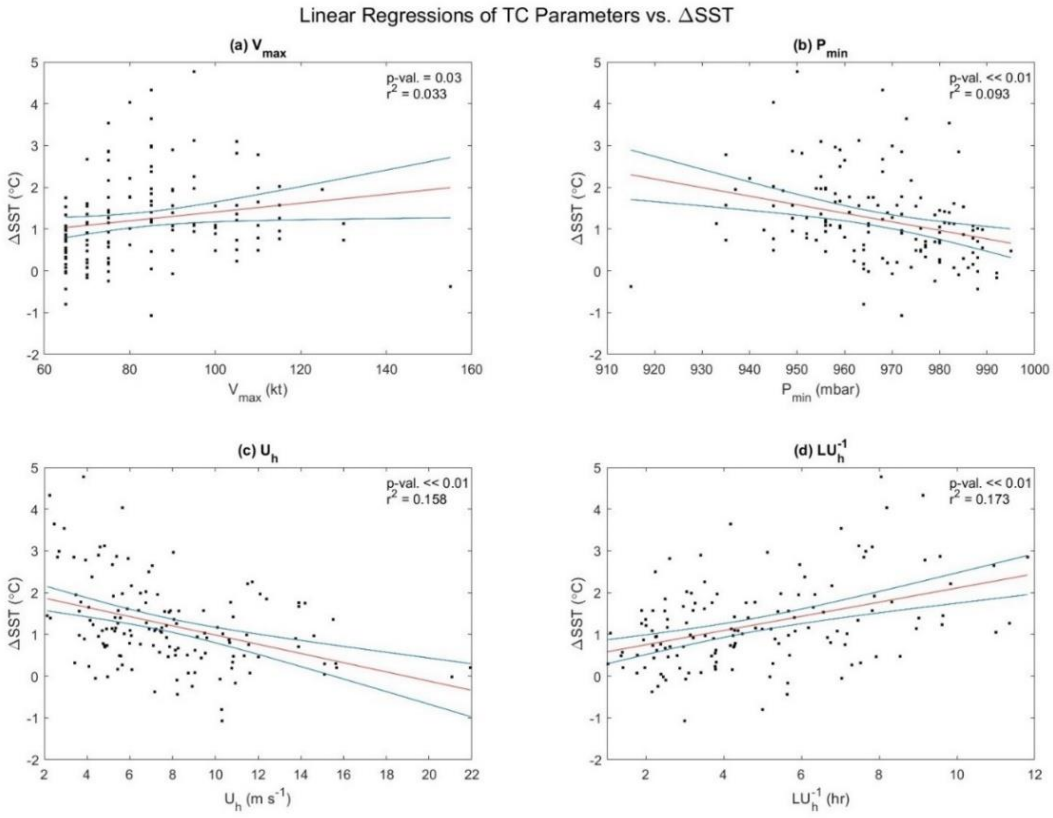

Figure 15: Linear regression of ΔSST with the statistically significant hurricane parameters (a) V_{max}, (b) P_{min}, (c) U_h, and (d) LU_h^{-1}. The red line represents the line of best fit, and the blue lines indicate the 95% confidence interval.

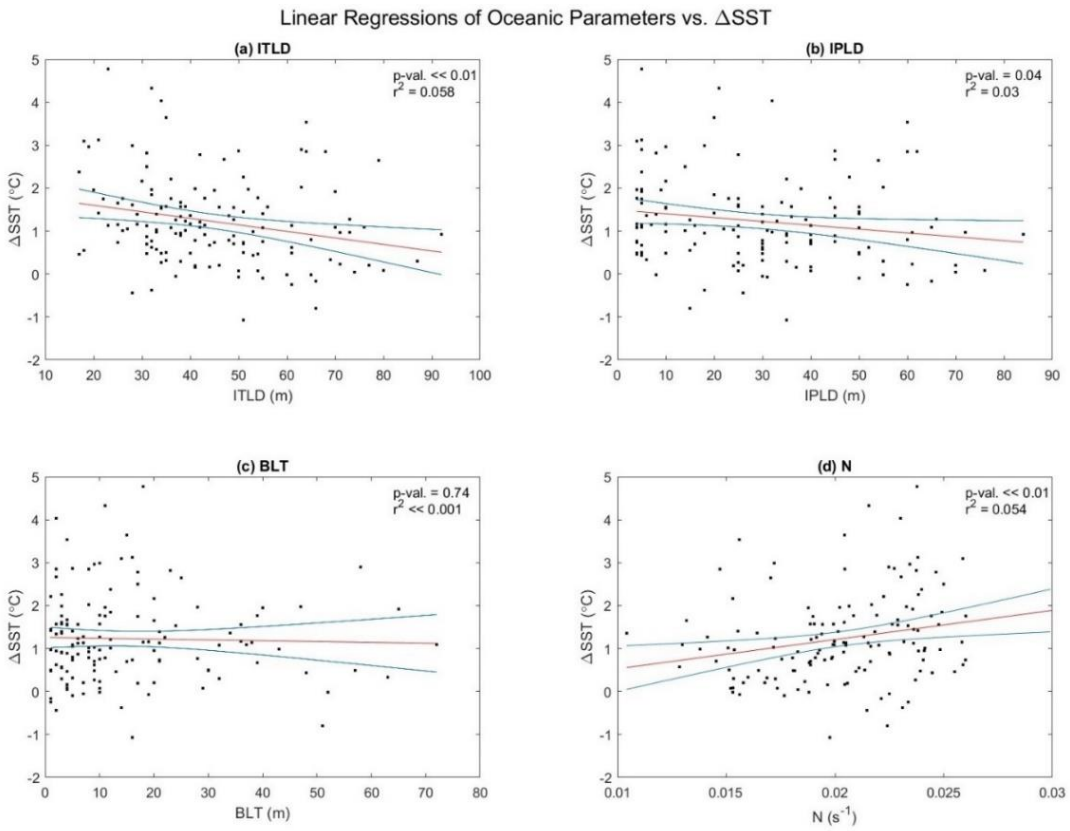

Figure 16: Linear regression of ΔSST with the oceanic parameters (a) ITLD, (b) IPLD, (c) BLT, and (d) N. The red line represents the line of best fit, and the blue lines indicate the 95% confidence interval.

4.2 Principal Component Analysis

A PCA was performed on a matrix containing *ΔSST*, P_{min}, LU_h^{-1}, *ITLD*, and *BLT*. To minimize potential overlap, only certain parameters were selected for this analysis. For instance, only one of the two metrics for hurricane strength was included in the matrix. Because P_{min} outperformed V_{max} in the linear regressions, it was retained for the PCA. Similarly, between the two MLD metric, *ITLD* outperformed *IPLD* and thus was chosen for the PCA. Regarding hurricane size and speed metrics, either LU_h^{-1} alone could have been included, or both U_h and *RMW* could have been included. Since LU_h^{-1} performed best of the three, it was selected.

Although results presented in the linear regression indicate *BLT* does not have a statistically significant relationship with *ΔSST*, it was retained for the PCA because it has been previously shown to be a metric that can influence hurricane-included oceanic cooling (Haakman et al., 2019).

Figure 17 shows the percentage of variance explained by all five modes of the PCA. Mode 1 is able to explain 31.8% of the variance, with the first three modes combining to explain 77.1%. Table 4 shows the loading values for each individual parameter for all five modes of the PCA. Mode 1 described the relationship between *ΔSST*, P_{min}, LU_h^{-1}, and *ITLD*. Principally, high mode 1 scores refer to conditions where significant cooling resulted from a strong hurricane that had a considerable amount of time to generate mixing in the upper ocean, and a shallow isothermal layer beneath the storm. Mode 2 describes the relationship between *ΔSST*, P_{min}, *ITLD*, and *BLT*. High mode 2 scores refer to conditions where some cooling occurred to the presence of an exceptionally powerful hurricane over a thick barrier layer and a deep isothermal layer.

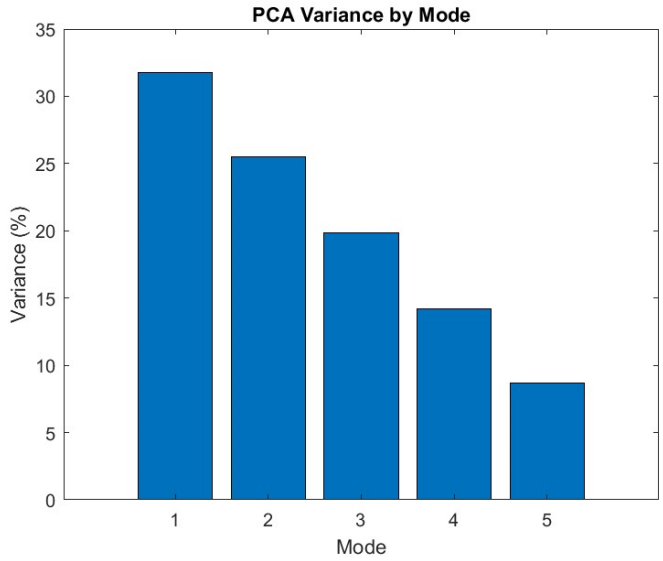

Figure 17: The percentage of total variance explained by all five modes of the PCA.

Table 4: The loading values of each parameter for all five modes of the PCA.

Parameter	Mode 1	Mode 2	Mode 3	Mode 4	Mode 5
ΔSST	0.68	0.17	0.05	0.02	0.71
P_{min}	-0.29	-0.63	0.36	0.49	0.39
LU_h^{-1}	0.52	-0.11	0.65	0.11	-0.53
$ITLD$	-0.38	0.32	0.66	-0.50	0.26
BLT	-0.17	0.68	0.12	0.70	-0.03

Similar to mode 1, mode 3 describes the relationship between ΔSST, P_{min}, LU_h^{-1}, and *ITLD*. High mode 3 scores refer to conditions where a strong hurricane with ample time to mix the upper ocean while translating over a deep isothermal layer had no effect on oceanic cooling. Similar to mode 2, mode 4 describes the relationship between ΔSST, LU_h^{-1}, *ITLD*, and *BLT*. High mode 4 scores refer to conditions where an intense hurricane translating over a shallow isothermal layer and deep barrier layer also has no impact on oceanic cooling. Lastly, mode 5 describes the relationship between ΔSST, P_{min}, LU_h^{-1}. High mode 5 scores refer to conditions where significant cooling occurred under a weak hurricane that had minimal time to mix the upper ocean.

Figures 18 and 19 offer a visual comparison of different mode scores versus one another. Figure 18 shows the scatter plot of mode 1 scores versus mode 2 two scores, color coded by hurricane category. From this figure, it can be seen that category-1 and category-2 hurricanes cover the full range of mode 1 scores, although category-1 hurricanes are more concentrated towards the lower scores. Major hurricanes, particularly category-4 and category-5 storms, have little variation in mode 1 scores and are concentrated near the center. Regarding mode 2, it appears that scores increase with hurricane category, with the exception of a handful of category-2 and category-3 hurricanes claiming the highest mode 2 scores.

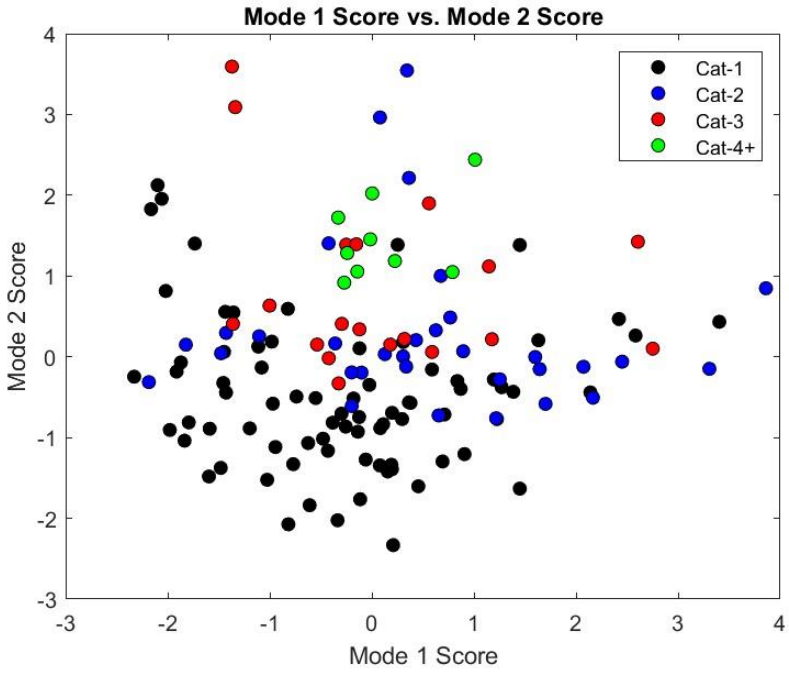

Figure 18: Scatter plot of mode 1 and mode 2 scores from the PCA, color coded by hurricane category.

Similarly, Figure 19 is a scatter plot of mode 3 versus mode 4 scores, color coded by hurricane category. Unlike modes 1 and 2, less obvious trends exist with modes 3 and 4. This is more apparent with the minor hurricanes, as category-1 and category-2 storms cover a wide range of scores across both modes. The only exception to this potentially being that category-1 hurricanes are slightly shifted towards having higher mode 3 scores. More identifiable trends exist for major hurricanes, and with category-4 and category-5 storms in particular. Major hurricanes appear to have lower scores across both modes, with this trend being more apparent in high category hurricanes, with the only category-5 hurricane in this dataset toting the lowest mode 3 score, and one of the lowest mode 4 scores.

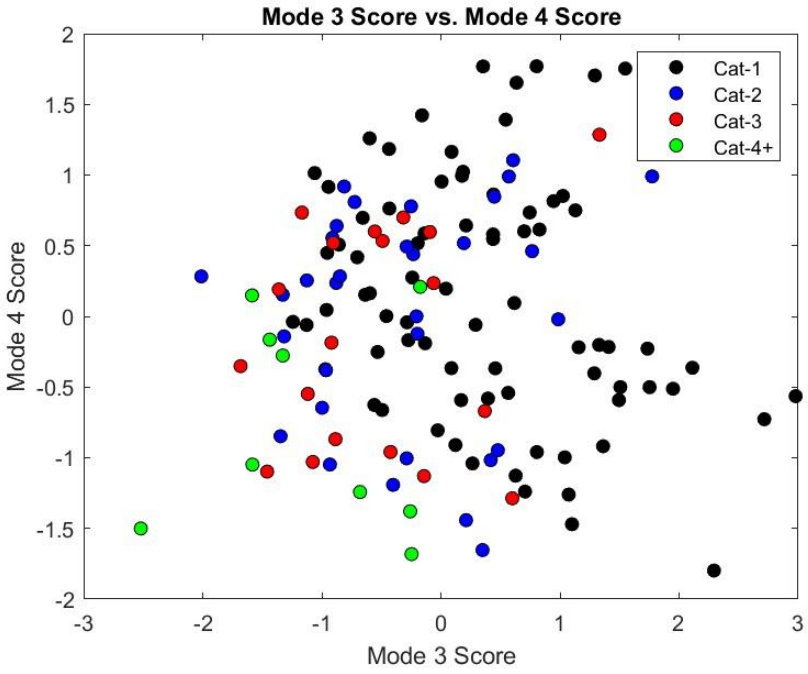

Figure 19: Scatter plot of mode 3 and mode 4 scores from the PCA, color coded by hurricane category.

Additional analyses of the scores from PCA modes came in the form of ANOVA tests to look for statistically significant differences among across different months. The box and whisker plots of the ANOVA tests for the scores of mode 1, mode 2, mode 3, mode 4, and mode 5 are shown in Figure 20. Of the five modes, three yielded statistically significant p-values. This included mode 1, mode 4, and mode 5 with p-values of 0.04, <<0.01, and 0.03 respectively. Although the ANOVA tests revealed statistically significant p-values for mode 1 and mode 5, multiple comparisons tests showed there were no statistically significant differences in scores between any of the months. A multiple comparisons test of mode 4 revealed that scores were statistically different between October and July, and October and August. The p-values for mode 2 and mode 3 scores were 0.44 and 0.34 respectively, and multiple comparisons also revealed no significant differences in mode scores between months. Regardless of p-values, the box and

whiskers plots for each of these modes indicate some identifiable trends between mode scores and months that will be touched upon in the discussion.

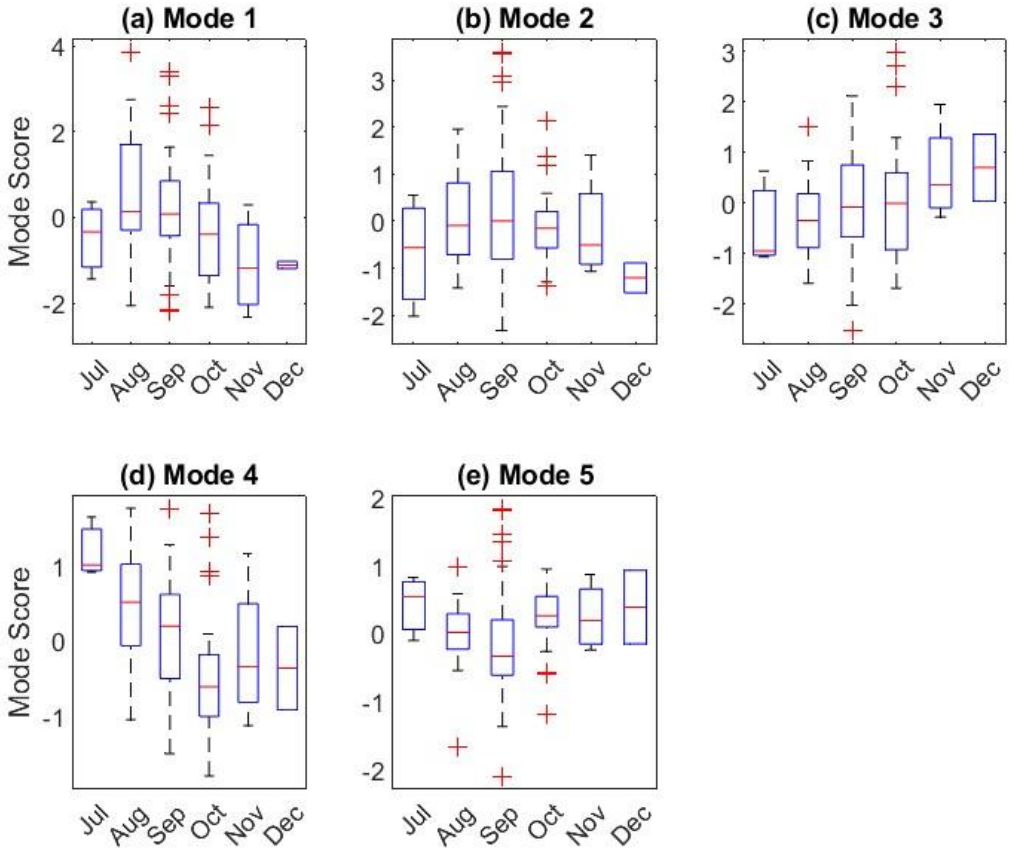

Figure 20: Box and whiskers plot for the results of the ANOVA test of mode scores binning by month for (a) mode 1, p-value = 0.04, (b) mode 2, p-value = 0.44, (c) mode 3, p-value = 0.34, (d) mode 4, p-value << 0.01, and (e) mode 5, p-value = 0.03. Red lines show the median cooling value for each month. Horizontal blue lines on each box represent the 25th and 75th percentile values. Horizontal black lines show the maximum and minimum values that are not considered outliers. Red crosses are outlier values.

4.3 Analysis of Variance on Oceanic cooling

ANOVA tests were performed on ΔSST to try and identify statistically significant differences in oceanic cooling between different months and hurricane categories on the

SSHWS. Figures 21 and 22 show the box and whiskers plots of these ANOVA tests for months and hurricane category respectively. Of the two, only the ANOVA test on *ΔSST* binning by hurricane category yielded a statistically significant result. A multiple comparisons tests revealed there are statistically significant differences in *ΔSST* between category-1 and -2 hurricanes, with category-2 hurricanes causing greater cooling. The ANOVA test on *ΔSST* binning by month yielded a p-value of 0.5 meaning there is no statistically significant difference in oceanic cooling between different months.

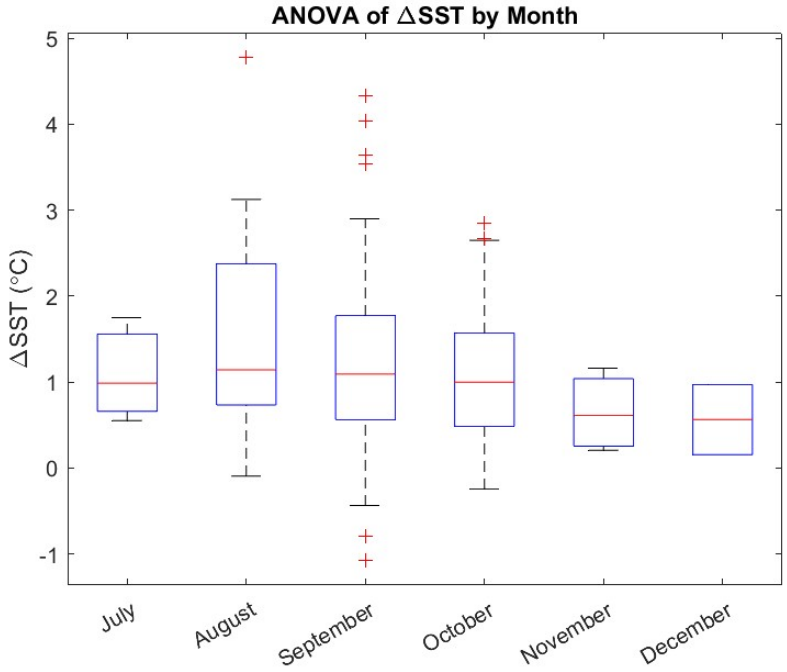

Figure 21: Box and whiskers plot for the results of the ANOVA test of ΔSST binning by month. Horizontal blue lines on each box represent the 25th and 75th percentile values. Horizontal black lines show the maximum and minimum values that are not considered outliers. Red crosses are outlier values. P-value = 0.5.

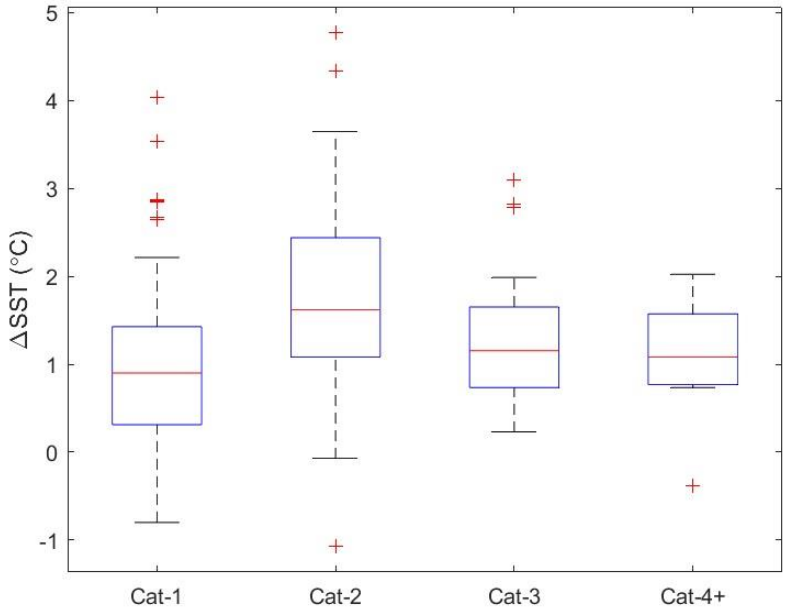

Figure 22: Box and whiskers plot for the results of the ANOVA test of ΔSST binning by hurricane category. Red lines show the median cooling value for each month. Horizontal blue lines on each box represent the 25th and 75th percentile values. Horizontal black lines show the maximum and minimum values that are not considered outliers. Red crosses are outlier values. P-value << 0.01.

4.4 Multilinear Regression

The fourth method of statistical analysis was MLR. In an attempt to better predict *ΔSST*, a MLR model was developed using the fewest number of parameters that could explain the most variation in *ΔSST*. Figure 23 shows the percentage of variance explained in *ΔSST* from r^2 values using MLR models constructed using a variety of the parameters in Table 2. Six MLRs were performed on *ΔSST*, each with an additional predictor parameters included. Parameters were added based on their r^2 values from the single linear regressions, with those that could explain the most variance in *ΔSST* being selected first. Additionally, some parameters were not included as to avoid overlap (e.g., P_{min} instead of V_{max}, *ITLD* instead of *IPLD*). The first MLR, technically a single linear regression, contained one predictor parameter, LU_h^{-1}. LU_h^{-1} was chosen as the first

parameter because based on the linear regressions, it was the single parameter that could explain the most variation in ΔSST (17.3%). The second MLR includes LU_h^{-1} and P_{min} as predictor variables and can explain 27.4% of the variation in ΔSST. For the third, *ITLD* is added and the MLR explains 32.1% of the variation in ΔSST. The fourth, fifth, and sixth MLRs added *BLT*, then *N*, and finally Lat_{TC}, respectively, and explain 32.1%, 32.3%, and 32.4% of the variation in ΔSST. Because of the minimal increase in variance explained in the fourth, fifth, and sixth MLRs, the third is used to construct the MLR model with the equation:

$$\Delta SST_{predict} = 21.34 + 0.17(LU_h^{-1}) - 0.021(P_{min}) - 0.014(ITLD)$$

where $\Delta SST_{predict}$ is the predicted ΔSST value based on the input of data for the predictor parameters.

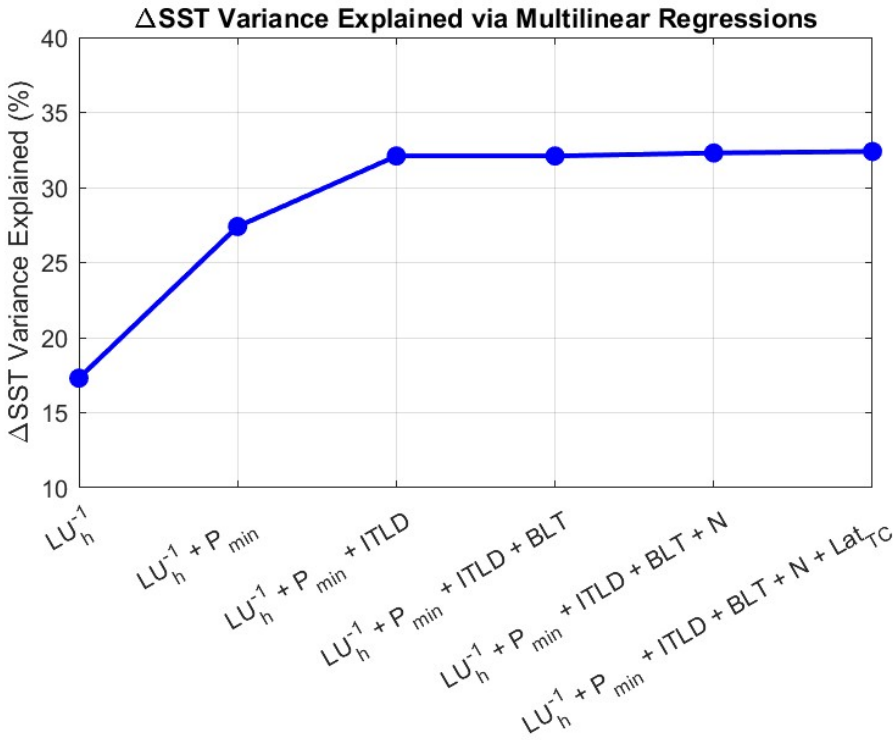

Figure 23: The percentage of variance explained in ΔSST from MLR models containing increasing numbers of predictor parameters.

For comparison, Figure 24 shows a scatter plot of ΔSST values versus $\Delta SST_{predict}$ values using real data plugged into the equation above. While there is still some agreement, it is clear that a considerable amount of variability remains in $\Delta SST_{predict}$. The average difference between ΔSST and $\Delta SST_{predict}$ values is small at 0.006 ℃, however, the standard deviation is 0.8 ℃. Furthermore, there are clear differences in the range of values between ΔSST and $\Delta SST_{predict}$. The minimum and maximum ΔSST values from this study are -1.1 ℃ and 4.8 ℃ respectively, resulting in a range of 5.8 ℃. Comparatively, the minimum and maximum values of $\Delta SST_{predict}$ are -0.1 ℃ and 2.8 ℃, yielding a range of just 2.9 ℃.

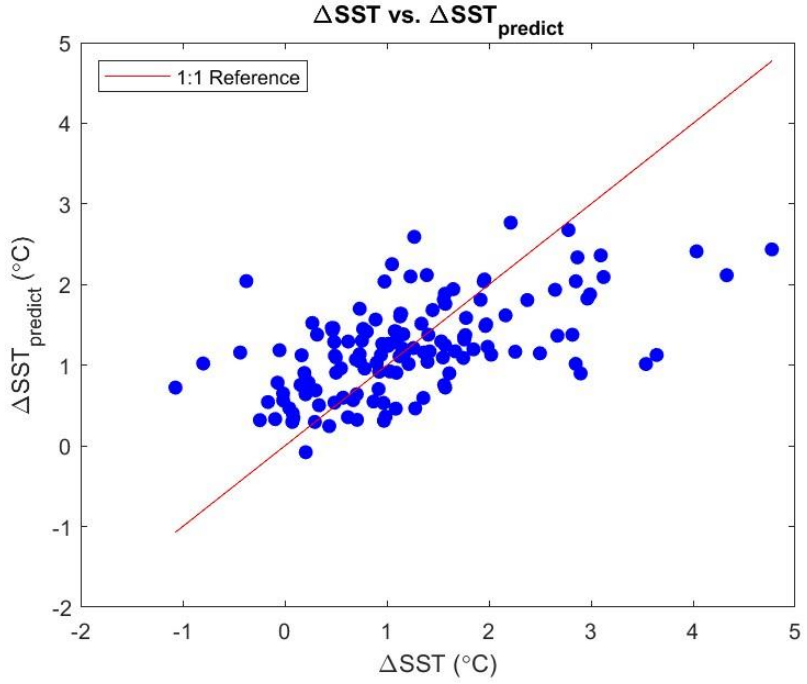

Figure 24. Scatter plot of ΔSST versus $\Delta SST_{predict}$ from the 2xRMW MLR with predictor parameters LU_h^{-1}, P_{min}, and $ITLD$. Blue circles indicate scattered data and the red line is a 1:1 reference.

5. DISCUSSION

5.1 Discussion of Linear Regression

Linear regressions reveal that select hurricane parameters have a larger contribution to oceanic cooling than each oceanic parameter considered. Focusing on 2xRMW from Table 2, the two parameters that can explain the most variance in ΔSST are hurricane parameters. This includes LU_h^{-1} (a function of hurricane size and translation speed) which explains the most variance in ΔSST, and P_{min} (a function of hurricane strength) which explains the second-most variance. The parameters that explain the third- and fourth-most variance in ΔSST are oceanic, *ITLD* and *N*, respectively. The two remaining parameters with statistically significant relationships with ΔSST are V_{max} and *IPLD*. Disregarding *RMW* because it is considered in LU_h^{-1}, the two parameters that do not have statistically significant relationships with ΔSST and explain the least variance are Lat_{TC} and *BLT*.

The trends present at 2xRMW also exist at 3x and 4xRMW, however, each parameter generally explains less variance at greater distances. As with 2xRMW, the parameters with statistically significant relationships with ΔSST at 4x and 3xRMW are LU_h^{-1}, P_{min}, *ITLD*, *N*, V_{max}, and *IPLD*, with Lat_{TC} and *BLT* remaining insignificant yielding p-values above 0.4. Between 4x and 3xRMW, there is minimal difference in the percentage of variance explained in ΔSST. From 4x to 3xRMW, the percentage of variance explained in ΔSST for LU_h^{-1} and P_{min} increases by 2.2% and 0.3% respectively. However, moving from 3x to 2xRMW, these values increase by 5% and 2.8% respectively. With *ITLD* and V_{max}, there are actually decreases in the percentage of variance explained in ΔSST from 4x to 3xRMW. These decreases are 0.8% for *ITLD* and 0.2% for V_{max}. As with LU_h^{-1} and P_{min}, there are noticeable increases in these values moving from 3x to

2xRMW. In these scenarios, the percentage of variance explained in *ΔSST* increased by 1.3% for *ITLD* and 1% for V_{max}. The trend of less variance explained at further distances is intuitive, because at some distance from the hurricane center the system will have no impact on the ocean. Based on data from 2x to 4xRMW, it seems there is a substantial decrease in the contribution of these parameters at distances greater than 2xRMW. When attempting to utilize hurricane and oceanic data to predict oceanic cooling, a higher level of accuracy can be achieved if the data used are within 2xRMW.

Results from 1xRMW vary greatly in comparison to those from 2x, 3x, and 4xRMW. At 1xRMW, just two parameters had statistically significant relationships with *ΔSST*: LU_h^{-1} and P_{min}, with LU_h^{-1} explaining 27.1% of the variance in *ΔSST* and P_{min} explaining 16%. From 2x to 1xRMW the percentage of variance explained in *ΔSST* for these parameters increases by 9.8% and 6.7% respectively. *ITLD*, the parameter that can explain the most variance in *ΔSST* of all oceanic parameters considered, had a significant decrease in variance explained from 2x to 1xRMW, decreasing by 3.4%. In this study, just 38 data points are present within 1xRMW which could potentially lead to findings that may not fully encompass the relationship between the parameters of interest and *ΔSST* within 1xRMW. Considering data from 4x to 1xRMW, these values support the importance of utilizing hurricane data closer to the hurricane center to achieve the best predictions of oceanic cooling, and ultimately forecasting of hurricane intensity.

In all four scenarios, the hurricane parameters LU_h^{-1} and P_{min} are able to explain the most variance in *ΔSST*, supporting *Hypothesis One* that hurricane parameters have a greater impact on oceanic cooling than oceanic parameters. As such, accurate measurements of hurricanes parameters, principally strength and translation speed, should be prioritized in predictions of oceanic cooling. Data from these linear regressions also support *Hypothesis Three*, which stated

that hurricane parameters will have a greater influence on ΔSST closer to the hurricane center. As the data is limited to those closer to the hurricane center, LU_h^{-1} is consistently able to explain more variance in ΔSST indicating it has a greater contribution to oceanic cooling closer to the hurricane center. This is also the case for P_{min}. Although there was a minimal decrease in the percentage of variance explained in ΔSST between 4x and 3xRMW (6.5% to 6.2%), there is a considerable increase from 2x to 1xRMW (9.3% to 16%). Although it explains less variance than LU_h^{-1} and P_{min}, this trend also existed with V_{max}. At 4x, 3x, 2x, and 1xRMW, V_{max} explains 2.5%, 2.3%, 3.3%, and 7.5% of the variance in ΔSST respectively. This supports the notion that hurricanes parameters can explain a greater amount of variance in ΔSST closer to the hurricane center, particularly within 2xRMW.

Hypothesis Three also stated that oceanic parameters would become more important further from the hurricane center. However, this does not appear to be the case. For the oceanic parameters considered, there were either minimal differences in r^2 values from 4x to 1xRMW, or increases from the 4x to 1xRMW as with the hurricane parameters. Beginning with *ITLD* because it is the most important oceanic parameter to ΔSST, it explains 5.3%, 4.5%, 5.8%, and 2.4% of the variance in ΔSST at 4x, 3x, 2x, and 1xRMW respectively. These values reveal no clear trend in the contribution of *ITLD* at varying distances from the hurricane center. Thus, if taking the three most important parameters LU_h^{-1}, P_{min}, and *ITLD* into consideration, any differences in the percentage of variance explained in ΔSST between different datasets (varying distances from the hurricane center) can only really be attributed to the hurricane parameters. The other two oceanic parameters with statistically significant relationships with ΔSST (*IPLD* and *N*), had similar trends to the hurricane parameters in that r^2 generally increased moving closer to the hurricane center. Moving from 4x to 1xRMW, *IPLD* explains 2.3%, 2.3%, 3%, and

7% of the variance in ΔSST respectively. From 4x to 1xRMW, N explains 3.7%, 3.6%, 5.4%, and 6% of the variance in ΔSST.

Within Table 2, there are two parameters used to define hurricane strength: P_{min} and V_{max}. V_{max} is often the preferred metric for conveying the strength of a hurricane. The NHC, Japan Meteorological Agency, Fiji Meteorological Service, and India Meteorological Department all classify TCs into categories solely based on variations of V_{max}. The results of the linear regressions in this study indicate that for cooling beneath hurricanes, P_{min} is consistently a better metric than V_{max}. At 1x, 2x, 3x, and 4xRMW, P_{min} explains over twice as much variance in ΔSST as V_{max}. One reason for this difference could be due to the accuracy in measurements of both V_{max} and P_{min}. Measurements of V_{max}, particularly those obtained through aircraft reconnaissance, tend to much more variable in comparison to P_{min} measurements from aircraft reconnaissance or dropsondes (Rosendal, 1982). As such, P_{min} values being more reliable than those for V_{max} is one possible explanation as to why P_{min} exhibits a stronger statistical relationship with ΔSST compared to V_{max}. Until more reliable V_{max} values can be obtained within hurricanes, P_{min} appears to be the best strength metric in relation to oceanic cooling, and therefore may be more useful in predicting changes in hurricane intensity.

Also within Table 2 are two separate metrics of MLD, *ITLD* and *IPLD*. At 4x, 3x, and 2xRMW, *ITLD* outperformed *IPLD* in explaining more variance in ΔSST. Although *IPLD* outperformed *ITLD* at 1xRMW, it should be noted that p-vales of these linear regressions with ΔSST were both greater than 0.05 (0.35 for *ITLD* and 0.11 for *IPLD*). Thus, it appears that the *ITLD* is better metric for determining oceanic cooling than *IPLD*. One possible explanation is that *ITLD* is a function of temperature while *IPLD* is a function of density. Because ΔSST is a measure of changes in surface temperature, the temperature defined mixed layer depth *ITLD* may

be expected to have a stronger correlation with *ΔSST* than the density defined mixed layer depth *IPLD*.

The results of the linear regressions of *N* with *ΔSST* in all four datasets produced interesting results. At 4x, 3x, and 2xRMW, *N* has a statistically significant relationship with *ΔSST*, with r^2 values inferring that it is the fourth-most important parameter in predicting *ΔSST*, and the second-most important oceanic parameter behind *ITLD*. Although the p-value for *N* at 1xRMW is not statistically significant, the r^2 value still denotes some importance (remains fourth-most parameter and second-most important oceanic parameter). Focusing on data at 4x, 3x, and 2xRMW because of the statistical significance, the results are interesting because the trend of the linear regressions suggests that greater cooling occurs when *N* is larger, or more simply, when the water column is strongly stratified. This result is counterintuitive because on a fundamental level, increased stratification in the water column limits the vertical mixing of water masses (Guancheng et al., 2020). Therefore, the expected result would be greater cooling in situations where *N* is small, or when stratification is weak and vertical mixing is more likely to ensue.

However, there are two main effects that stratification can have on oceanic cooling, only one of which is described above. While the first relates to physical mechanisms causing vertical mixing and subsequent cooling (or lack thereof), the second is founded on thermodynamics. When a water column experiences strong stratification, there is generally a large temperature difference between the surface and depth. In this scenario, for the same level of vertical mixing, there is a greater transfer of heat from surface to depth in more stratified waters resulting in an enhanced observed cooling at the sea surface. Therefore, in circumstances where there is stratification with a considerably large vertical temperature gradient, surface cooling can occur

even if vertical mixing from atmospheric forcing is limited. The results of the linear regressions suggest that although vertical mixing from surface forcing was reduced due to increased stratification denoted by larger *N* values, surface cooling was still observed and could potentially be due to an enhanced transfer of heat downward from the surface to depth.

5.2 Discussion of Principal Component Analysis

5.2.1 Discussion of Mode Scores

The PCA gives a closer look at which parameters work together to moderate oceanic cooling. In mode 1 of the PCA at 2xRMW which has a significantly large loading value for ΔSST (0.68), the parameter with the strongest loading value is the hurricane parameter LU_h^{-1}, with a value of 0.52. Following this is the oceanic parameter *ITLD* with a loading value of -0.38. This result indicates that in situations where significant oceanic cooling occurs, the hurricane has a substantial time to mix the upper ocean in addition to the vertical mixing not having to occur as deep due to the presence of a shallow isothermal layer. Furthermore, a long LU_h^{-1} and a shallow *ITLD* contribute more to oceanic cooling than the storm strength P_{min} which has a loading value of -0.29 in mode 1. The largest mode 1 score from the dataset is 3.86. This datapoint represents a scenario where an oceanic cooling of 4.8 ℃ occurred beneath a hurricane with a P_{min} of 950 mbar, an LU_h^{-1} eight hours, and over an *ITLD* of 23 m. For comparison, the average ΔSST, P_{min}, LU_h^{-1}, and *ITLD* values from this dataset are 1.2 ℃, 967 mbar, five hours, and 44 m respectively. These results generally support *Hypothesis Two* in that greater cooling occurs under strong hurricanes translating over shallower isothermal layers with ample time to generate mixing beneath them. Results from this mode also align with the linear regressions, with the only difference being greater emphasis placed on *ITLD* than P_{min}. This mode, which can explain the most variance, confirms that LU_h^{-1} has the strongest relationship with ΔSST, and that P_{min} and

ITLD are also of importance and should be taken into consideration for predictions of ΔSST and changes in hurricanes intensity.

In mode 2 of the PCA in which there is a moderate cooling response (ΔSST loading value = 0.17), P_{min} is the dominant hurricane parameter (loading value = -0.63). Interestingly, the strongest loading value of all is 0.68 for *BLT*. The third most important parameter in this mode is *ITLD* with a loading value of 0.32. These results indicate that some degree of cooling may still occur where a powerful hurricane translates over a large barrier layer and deep isothermal layer. On a fundamental level, a larger barrier layer and deep isothermal layer are not conducive for oceanic cooling as greater vertical mixing would be required to stir up cooler waters from below. The highest mode 2 score is 3.59, associated with a stronger hurricane (P_{min} = 957 mbar) that translated over a large barrier layer (*BLT* = 72 m) and deep isothermal layer (*ITLD* = 76 m) that caused a cooling of 1.1 ℃. For comparison, the average *BLT* in this dataset is 15 m. Here, the scenario with the highest mode 2 score actually resulted in a less than average cooling. Even though the hurricane was stronger than average, the cooling response was likely mitigated by the very thick barrier layer and deep isothermal layer. Taking a step back to examine the entire dataset, because there is a considerably strong loading value for P_{min}, it can be inferred that significantly powerful hurricanes can overcome large barrier layers and deep isothermal layers to still yield some amount of cooling. It is important to note that when LU_h^{-1} is less important as inferred from its loading value of -0.11, the oceanic metrics *BLT* and *ITLD* can suppress the oceanic cooling beneath powerful hurricanes. In regard to ΔSST predictions and hurricane intensity forecasts, this mode emphasizes the importance of ocean metrics in addition to hurricane metrics. Even if the hurricane is powerful, if it does not have ample time to generate

mixing, the cooling response can be greatly suppressed by oceanic conditions such as a large barrier layer and a deep isothermal layer.

Mode 3 of this PCA tells of situations in which there was an insignificant cooling response (*ΔSST* loading value = 0.05). The contributing parameters to this mode are *ITLD*, LU_h^{-1}, and P_{min} with loading values of 0.66, 0.65, and 0.36 respectively. The interpretation of these mode scores is that even in situations where a hurricane has a considerably long time to mix the upper ocean, minimal cooling can occur if the hurricane is weaker and translating over a deep isothermal layer. Although results from the linear regression and mode 1 indicate that LU_h^{-1} is the most important parameter in regard to *ΔSST*, the results from mode 3 show that a long time to generate mixing can be balanced out by a deep isothermal layer, particularly if the hurricane is weaker. The highest mode 3 score from this dataset is 2.98. In this scenario, an oceanic cooling of 2.7 °C occurred beneath a hurricane with a P_{min} of 960 mbar, an LU_h^{-1} of 11 hours, and over an *ITLD* of 79 m. This event differs from the mode 3 loading values in that the hurricane in this case was stronger than average and caused a greater than average cooling. Here, a stronger hurricane with a considerable amount of time to generate upper ocean mixing was able to overcome a deep isothermal layer to produce an oceanic cooling value in the 88th percentile. The results from this individual hurricane highlight the importance of the hurricane parameters LU_h^{-1} and P_{min} over oceanic parameters like *ITLD*. However, taking the entire dataset into consideration, loading values support the notion from mode 2 in that while oceanic parameters may be less important than hurricane parameters on an individual level (as in the linear regressions), they must still be taken into consideration as deep isothermal layers appear to balance out hurricanes with long times to generate mixing in order to suppress cooling, especially in circumstances where the hurricane is weaker.

Mode 4 is another mode which tells of situations with minimal cooling responses (ΔSST loading value = 0.02). This mode is controlled by *BLT*, *ITLD*, and P_{min} with loading values of 0.7, -0.5, and 0.49 respectively. In circumstances where there is a shallow isothermal layer, insignificant cooling can occur if the hurricane is weak and the barrier layer is large. The highest mode 4 score from the dataset is 1.77, and is associated with a weaker hurricane (P_{min} = 987 mbar) that translated over a shallower isothermal layer (36 m) and deeper barrier layer (32 m) causing an oceanic cooling of 1.1 °C. Even though the *ITLD* is close to average, this example still supports the overall interpretation of the mode. A considerably weaker hurricane translating over a large barrier layer is unable to produce a strong cooling response, even if the isothermal layer is shallower than average. Conversely, a powerful hurricane translating over a thin barrier may produce no noticeable cooling in the presence of a deep isothermal layer. As with modes 2 and 3, and mode 3 in particular, there is a balancing of hurricane and oceanic parameters that contribute to ΔSST, and a combination of hurricane and oceanic parameters should be considered in predictions of ΔSST and forecasts of hurricane intensity.

The final mode, mode 5, resulted in the largest ΔSST loading value of all modes (0.71). In this mode, the dominant parameters are LU_h^{-1}, P_{min}, and *ITLD* with loading values of -0.53, 0.39, and 0.26 respectively. These results indicate that substantial oceanic cooling can be observed in situations where a weak hurricane with minimal time to generate mixing is translating over a deeper isothermal layer. Interestingly, these are all circumstances which are not conducive for oceanic cooling. The highest mode 5 score from the dataset is 1.85. During this event, an oceanic cooling of 3.5 °C (96th percentile) occurred beneath a hurricane with a P_{min} of 982 mbar (82nd percentile) and LU_h^{-1} of seven hours (78th percentile) while translating over an *ITLD* of 64 m (85th percentile). The only metric that differs from the mode in this example is the LU_h^{-1} value

which is longer than average, when compared to the mode which suggests higher scores being associated with shorter LU_h^{-1} values. The overarching interpretation of the mode is that even under non-ideal circumstances (e.g., weak hurricane, minimal time to generate mixing, deep isothermal layer), a large cooling response can occur which is the opposite of the expected outcome. While this appears to not be the case the majority of the time, it is something that requires consideration when predicting *ΔSST* and needs addressing in future research studies. With *ΔSST* playing a considerable role in hurricane intensity forecasting, a *ΔSST* opposite of the expectation could greatly flaw hurricane intensity forecasts that utilize an expected value. There is great need to determine the parameters/mechanisms that can explain the remaining variance in *ΔSST*, as there are clearly other processes contributing to these cooling responses. It should be noted, however, that mode 5 is able to explain the least variance in *ΔSST* among all the modes (8.7%), and thereby much of this result could potentially be due to noise within the dataset.

5.2.2 Discussion of Mode Score Scattering

Further analysis of the PCA came through scatter plots of mode scores against one another, color coded by hurricane category. The first of these scatter plots includes mode 1 scores versus mode 2 scores as seen back in Figure 18. Starting with mode 1 scores, the main trend is the lack of deviation from the center score with increasing hurricane category. Minor hurricanes cover the full range of mode 1 scores, with category-1 hurricanes skewing towards lower scores. Comparatively, major hurricanes are much more concentrated around the center value, particularly category-4 and category-5 hurricanes. High mode 1 scores are those in which considerable cooling occurs as result of a stronger hurricane with ample time to generate mixing over a shallow isothermal layer. As supported by the linear regressions, this trend indicates that hurricane strength is not the utmost import factor relating to oceanic cooling, with the largest

mode 1 scores belonging to category-1, category-2, and category-3 hurricanes. Figure 25 takes this examination a step further by showing the scatter plot of mode 1 scores versus mode 2 scores, color coded by different parameters within the PCA. Figure 25a is color coded by ΔSST, with the trend being greater cooling values associated higher mode 1 scores. Of the remaining subplots, the clearest trend among mode 1 scores is in LU_h^{-1} (Figure 25b), with longer values also associated with higher mode 1 scores. While trends with mode 1 scores still exist within P_{min} (Figure 25c) and *ITLD* (Figure 25d), they are not as clear as that for LU_h^{-1}. Because of the emphasis placed on ΔSST in this mode, trends here support the notion that LU_h^{-1} is the best indicator of oceanic cooling beneath hurricanes.

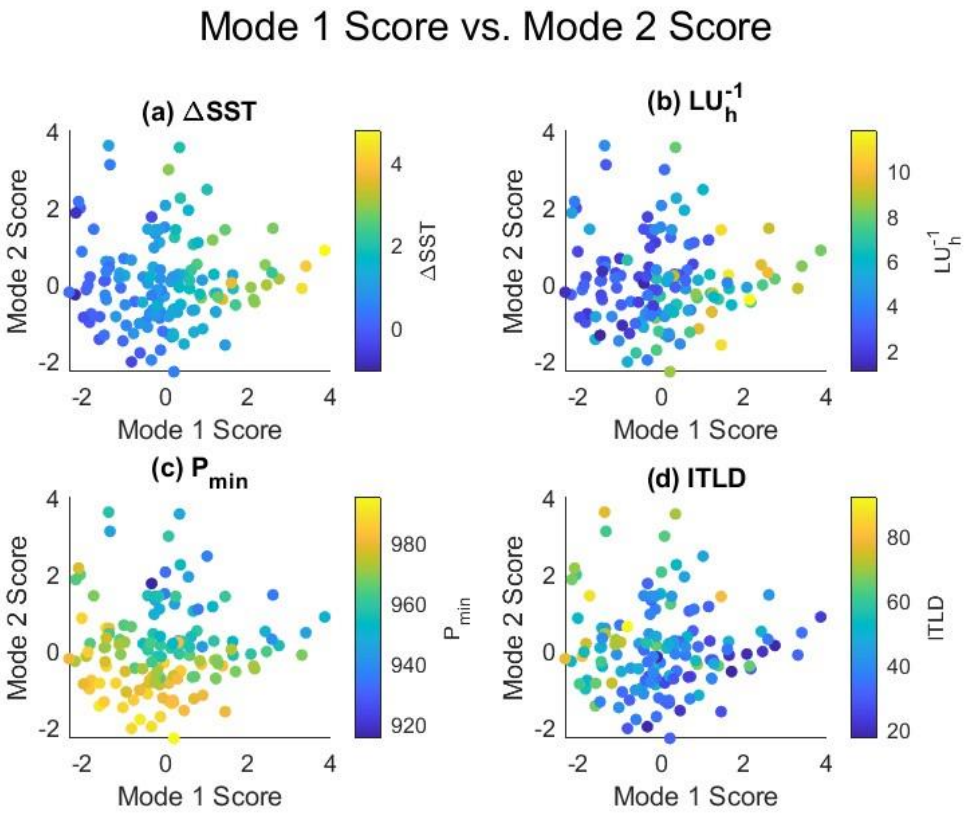

Figure 25: Scatter plots of mode 1 scores versus mode 2 scores from the PCA, color coded by (a) ΔSST, (b) LU_h^{-1}, (c) P_{min}, and (d) ITLD.

5.2.3 Discussion of Analysis of Variance on Mode Scores

ANOVA tests were performed on scores for each of the five modes to identify differences between months of the North Atlantic hurricane season. The box and whiskers plots of these tests are shown back in Figure 20. The ANOVA tests for scores from modes 1, 4, and 5 resulted in statistically significant p-values (p-value < 0.05). However, multiple comparisons tests revealed that only scores from mode 4 had statistically significant differences between at least two months. For this mode, there were statistically significant differences in scores between July and October and August and October, with July and August having higher scores than October. Although the other ANOVA tests and multiple comparisons tests did not reveal statistically significant differences between months for other mode scores, some interesting trends were still identifiable.

The box and whiskers plot of results from the ANOVA test for mode 1 scores by month is shown back in Figure 20a. This figure appears to show that mode 1 scores are low in July, peak in August, and decrease throughout the remainder of the season. The principal driving factor for this mode is LU_h^{-1}, followed by *ITLD* and P_{min}. Considering the large loading value for ΔSST, stronger cooling responses beneath powerful hurricanes with longer times to mix the upper ocean that are translating over shallow isothermal layers are more prevalent mid-season (August, September) than early (July) or in the late (October, November) to post-season (December). A closer look at the seasonality of LU_h^{-1} at 2xRMW revealed no discernable temporal trend. Breaking LU_h^{-1} apart, it appears that slower U_h values are concentrated in August and increase through November. However, no clear trend exists with *RMW* across the hurricane season. Looking at *ITLD*, trends show shallower values present earlier in the hurricane season that deepen moving into cooler months. This seasonal trend is often tied to calmer conditions and

subsequently less vertical mixing that occurs during summer months (Diaz et al., 2021). Data from 2xRMW reveal that the strongest hurricanes (those with lower P_{min} values) were most likely to occur in September, followed by August and October where hurricanes had similar strengths and frequencies. Ocean temperatures tend to be warmest around those months which may be a contributing factor to the increased likelihood of powerful hurricanes during that span. The cooling response is compounded by shallower isothermal layers that exist earlier in the season, allowing for relatively cooler waters to be stored closer to the sea surface. Furthermore, shorter LU_h^{-1} values contributing to this mode are driven by hurricane translation speed U_h more than hurricane size *RMW*. The observed seasonality of mode 1 scores where strong cooling occurs is mainly driven by shifts in hurricanes translation speed, depths of isothermal layers, and hurricane strength.

Figure 20b shows the box and whiskers plot of results of ANOVA scores by month for mode 2. Somewhat similar to mode 1, the trend here appears to show greater mode 2 scores mid-season (August, September) with lower scores in the early season (July) and late (October, November) to post-season (December). In this mode, the loading values indicate that some cooling occurs in the presence of large barrier layers, powerful hurricanes, and deep isothermal layers. Data from 2xRMW reveal no clear trend in *BLT* throughout the hurricane season, indicating that isothermal layers and isopycnal layers are possibly changing in similar increments throughout the season, as *BLT* is defined as the difference between these two metrics. It has previously been shown that isothermal layer depths and isopycnal layer depths change at comparable levels in the Gulf of Mexico, with both deepening as the hurricane season progresses (Potter & Rudzin, 2021). As mentioned with mode 1, warmer ocean waters present from August through October attribute to the development of stronger hurricanes, helping give rise to the

more powerful hurricanes that occur during these months. Also mentioned above, a clear seasonality trend exists for *ITLD*, with shallower depths occurring early in the season and deepening into the winter, which aligns with previous findings (Zhang et al., 2018). However, results from this mode indicate the occurrence of cooling in the presence of deep isothermal layers. Thus, the seasonality in mode 2 scores where some cooling occurs cannot be attributed to seasonal changes in isothermal layers. With no seasonal trend apparent in the barrier layers, the seasonality of mode 2 scores could be partially attributed to changes in hurricane intensity fostered by the seasonal changes in ocean temperature. In the presence of larger barrier layers and deeper isothermal layers, powerful hurricanes generated in the middle of hurricane season can still cause notable oceanic cooling.

The box and whiskers plot of the ANOVA test on mode 3 scores by month is presented back in Figure 20c. The trend in this figure appears to show progressively increasing mode 3 scores throughout the hurricane season. The lowest mode 3 scores are present in the early to mid-season (July, August) with the highest scores seen in the late (November) to post-season (December). High mode 3 scores indicate the presence of deep isothermal layers, long times to generate upper ocean mixing, and weaker hurricanes, with oceanic cooling being negligible. As mentioned with modes 1 and 2, 2xRMW data reveal shallower isothermal layers in the summer months which deepen moving into winter. The observed trend with LU_h^{-1} seems to be controlled by U_h, with slower hurricanes more prevalent in August as speeds increase throughout the season. Lastly, mid-season months have the strongest hurricanes, with this likely partially due to warmer ocean temperatures and increased tropical cyclone heat potential (TCHP) during this span. The higher mode 3 scores observed later in the hurricane season are likely being driven by the deepening of isothermal layers which mitigates any cooling response. Additionally, the

negligible cooling response may be due to the occurrence of weaker hurricanes (category-1), which are less able to generate mixing and cooling beneath them in comparison to category 2 through category-5 hurricanes. Contrary to the deeper isothermal layers and weaker hurricanes, the loading value indicating longer times to generate mixing is one that would result in greater cooling. The negligible oceanic cooling reflected in this mode is possibly due to the balancing of isothermal layer depths and hurricane strength with vertical mixing generation time. Early season observations where low mode 3 scores exist are potentially caused by relatively shallower isothermal layers and stronger hurricanes competing with a limited time to generate mixing compared to late-season conditions where deeper isothermal layers and weaker hurricanes balance longer times to generate mixing.

Results from the ANOVA test of mode 4 scores by month are shown in a box and whiskers plot back in Figure 20d. These appear to trend downward throughout the season, opposite of the trend that appeared for mode 3. The highest mode 4 scores are in July, at which point subsequent decreases occur moving into August, September, and October, followed by a slight increase in November with little to no change into December. This mode is dominated by *BLT*, followed by *ITLD* and P_{min} which have loading values of similar magnitude. More specifically, high mode 4 scores are associated with larger barrier layers, shallow isothermal layers, and weak hurricanes. Similar to mode 3, the loading value for ΔSST denotes negligible cooling under these conditions. With no discernable seasonal trend associated with barrier layers, the seasonality of this mode is likely controlled by both isotheral layer depth and hurricane strength. Although shallow isothermal layers, which are conducive for oceanic cooling, are present in the early season, the occurrence of large barrier layers combined with generally weaker hurricanes results in no identifiable cooling trend. Conversely, the low mode 4 scores

that occur later in the season are driven by deeper isothermal layers, stronger hurricanes, and smaller barrier layers. The interpretation here is that even in the presence of a stronger late season hurricane over a small barrier layer, oceanic cooling can be suppressed by the deepening of isothermal layers during these months.

Lastly, the box and whiskers plot of the ANOVA test on mode 5 scores are shown in Figure 20e. There does not appear to be any significant trend with these scores, although a decrease from July to September is visible with an increase in October that remains steady through December. Scores from July are similar to those in October, November, and December. Thus, the lowest mode 5 scores occur in August and September. Mode 5 has the largest loading value for ΔSST between all five modes, and it is driven by LU_h^{-1}, P_{min}, and $ITLD$. High mode 5 scores, where considerable cooling occurs, are associated with hurricanes that have less time to generate mixing, hurricanes that tend to be weaker, and deeper isothermal layers. As mentioned earlier, this makes for an interesting result as none of these conditions are conducive for mixing and oceanic cooling. Because higher mode 5 scores are present in the early and late hurricane season, the oceanic cooling that occurs in these typically less-active months must be attributed to parameters or mechanisms that were not considered in this study. The majority of results thus far have suggested that ideal conditions for oceanic cooling include powerful hurricanes with long times to generate mixing over shallow isothermal layers. In the case of August and September where low scores are present, scenarios that align with mode 5 indicate even under those circumstances, oceanic cooling can still be restricted.

5.2.4 Discussion of the Spatial Distribution in Mode Scores

Continuing with the PCA, there was interest in determining if any spatial pattern existed in mode scores throughout the North Atlantic basin. Of all five modes, only mode 2 scores

appear to have some visible spatial trend, with higher scores concentrated at lower latitudes. Figure 26 shows the spatial distribution of these scores in the North Atlantic basin. Figure 27a shows a linear regression run on mode 2 scores with Lat_{TC}. The linear regression yielded a p-value of << 0.01 and an r^2 value of 0.07, indicating there is a statistically significant relationship between mode 2 scores and Lat_{TC}. It can be inferred from this result that moderate cooling events resulting from powerful hurricanes over deep isotheral layers and thick barrier layers are more likely to occur at lower latitudes. To further identify the cause of this trend, linear regressions were performed on the main contributing parameters to mode 2 (*BLT*, P_{min}, and *ITLD*), in addition to V_{max}. Results from these linear regressions revealed that *BLT* (Figure 27d), P_{min} (Figure 27b), and V_{max} (Figure 27c) have statistically significant relationships with Lat_{TC}, with stronger hurricanes (lower pressures, higher wind speeds) and larger barrier layers occurring at lower latitudes. Between P_{min} and *BLT*, which were considered in the PCA, P_{min} has the strongest relationship with Lat_{TC} with a lower p-value, and a higher r^2 value of 0.062 compared to 0.029 for *BLT*. To further support this argument, a linear regression of the other hurricane strength metric, V_{max}, was included as well. This linear regression also yielded a statistically significant result, with an r^2 value of 0.234, indicating that 23.4% of the variance in a hurricane's maximum sustained wind speed could be attributed to the system's latitude. This trend could be partially due to the presence of warmer ocean waters at lower latitudes that support higher heat fluxes and hurricane intensification. These results support the notion that the observed relationship of higher mode 2 scores at lower latitudes is driven by the presence of more powerful hurricanes at lower latitudes, with some contribution from thicker barrier layers at lower latitudes as well.

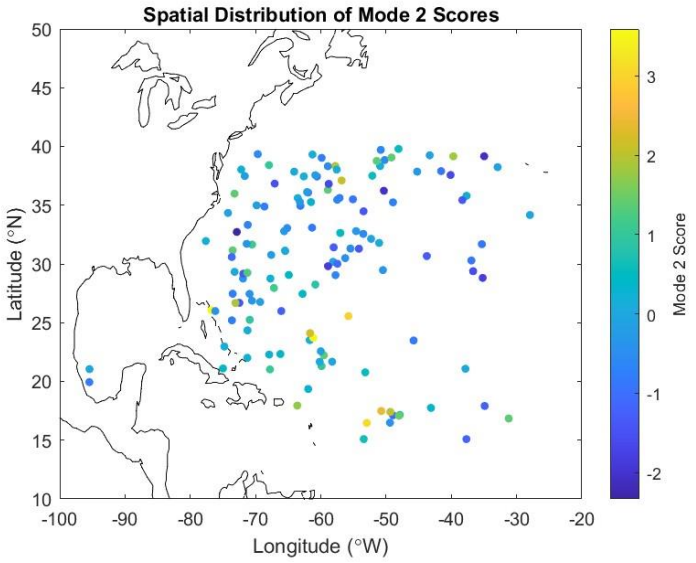

Figure 26: The spatial distribution of mode 2 scores from the PCA in the North Atlantic basin. Warmer colors denote higher scores and cooler colors denote lower scores.

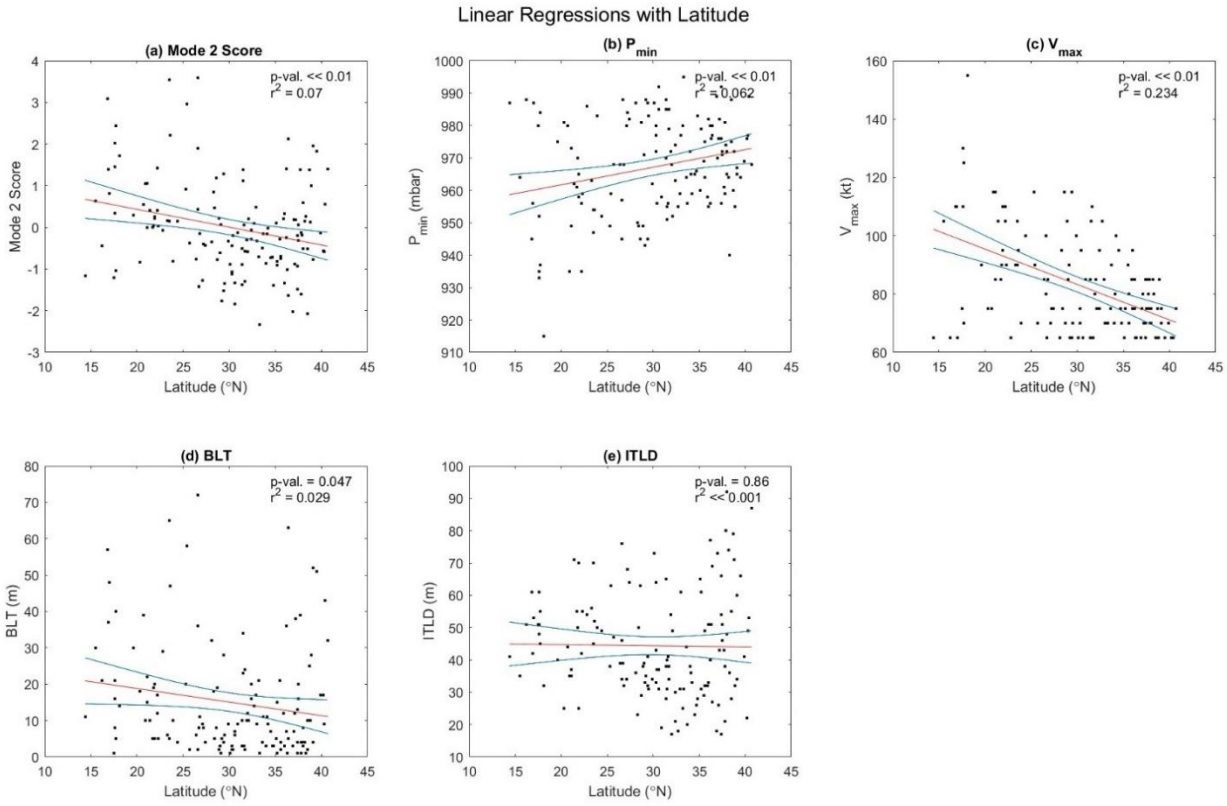

Figure 27: Linear regression of Lat_{TC} with (a) Mode 2 Score, (b) P_{min}, (c) V_{max}, (d) BLT, and (e) ITLD. The red line represents the line of best fit, and the blue lines indicate the 95% confidence interval. The p-value is << 0.01 and the r^2 value is 0.07.

For comparison, the spatial distribution of scores from modes 1, 3, 4, and 5 are shown in Figure 28. As mentioned above, no clear trends in spatial distributions appear with any of these modes. High mode 1 scores are associated with substantial cooling that is driven by powerful hurricanes with long times to generate mixing over shallow isothermal layers. The most important of these being high LU_h^{-1} values. In the 2xRMW data, there is no discernable spatial trend in LU_h^{-1}, however, some trends do exist with U_h and *RMW* individually. The spatial distributions of U_h and *RMW* can be seen in Figures 29a and 29b respectively. From these plots, it can be seen that the fastest hurricanes, as well as the largest, tend to be concentrated at higher latitudes, with slow-moving, smaller hurricanes more likely to occur at lower latitudes. This breakdown is likely the reason why there is not a strong spatial trend in LU_h^{-1}. At lower latitudes, longer times to generate mixing are driven by slow translation speeds but hindered by hurricanes being small. Comparatively, at higher latitudes, longer mixing times are controlled by larger hurricanes but hindered by fast translation speeds. The relationship between *RMW* and U_h is supported by a linear regression which yielded a p-value of $<< 0.01$ and an r^2 value of 0.128 (Figure 30). Increases in a hurricane's *RMW* are correlated with increases in translation speed. While LU_h^{-1} outperforms U_h and *RMW* in the linear regressions, these trends indicate that a greater emphasis may need to be placed on either U_h or *RMW* when predicting oceanic cooling beneath a hurricane.

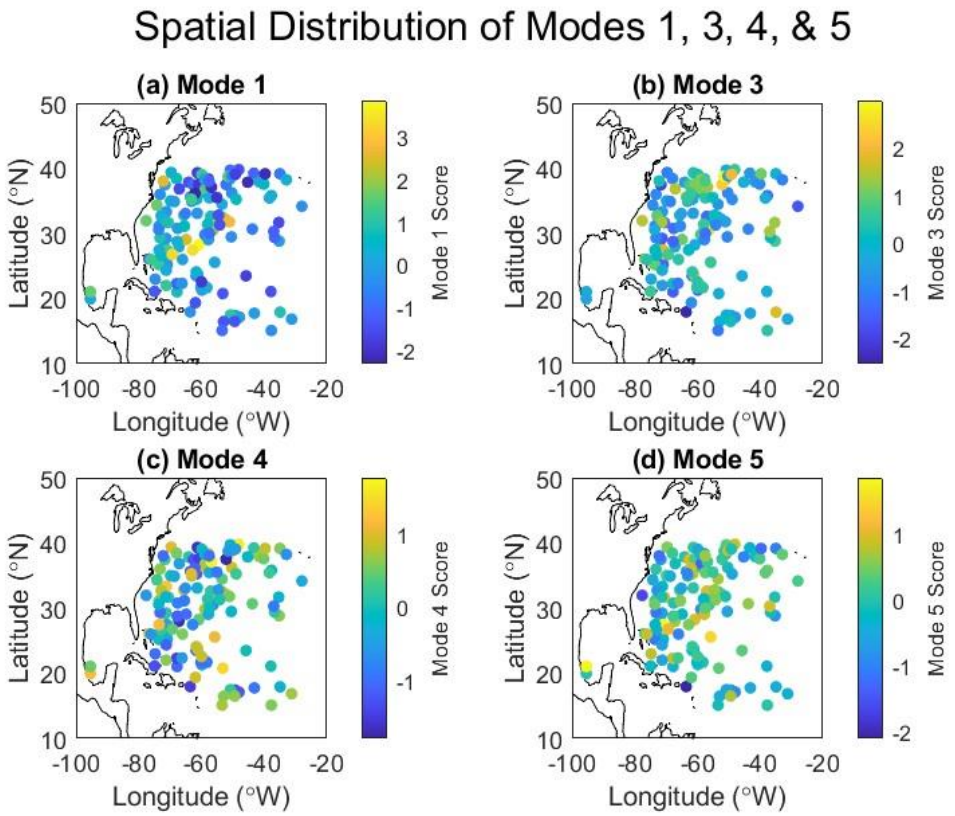

Figure 28: The spatial distribution of mode scores from the PCA for modes (a) 1, (b) 3, (c) 4, (d) and 5.

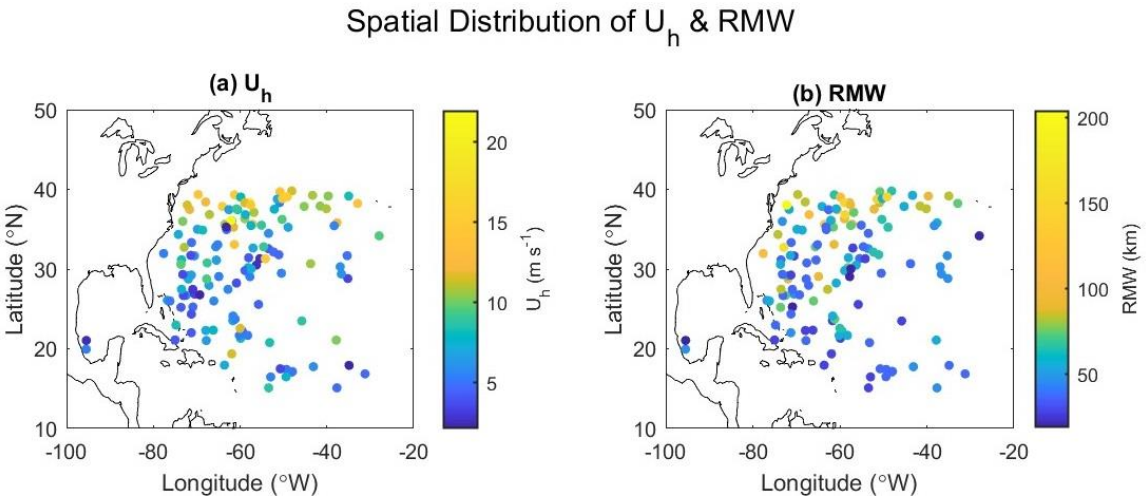

Figure 29. The spatial distribution of (a) LU_h^{-1} and (b) RMW.

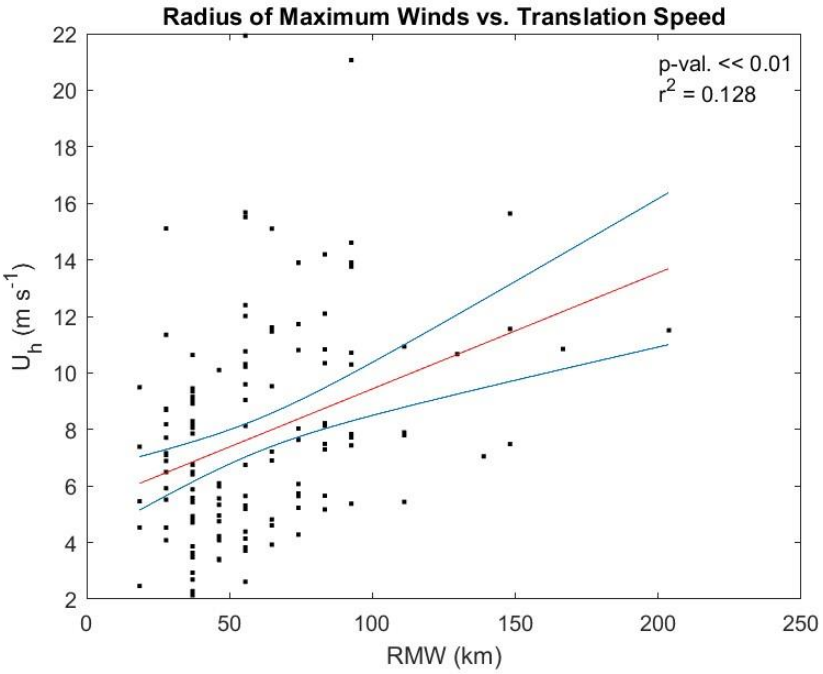

Figure 30. Linear regression of RMW with U_h. The red line indicated the line of best fit, while blue lines show the 95% confidence interval. P-value << 0.01.

5.2.5 Discussion of Mode Scores Across Datasets

The PCA results presented and discussed thus far pertain the primary dataset of interest, 2xRMW. Table 5 shows the loading values associated with the PCA parameters from all four datasets (4x, 3x, 2x, and 1xRMW) for comparison. For mode 1, there are no major differences in loading values for any parameter between at 4x, 3x, and 2xRMW. There are large loading values for ΔSST, with the LU_h^{-1} and *ITLD* acting as the two parameters with the greatest effect on ΔSST. However, at 1xRMW, the loading value for P_{min} decreases from -0.29 (2xRMW) to -0.49, with the *ITLD* loading value increasing from -0.38 to -0.02. Additionally, the loading value for *BLT* increases from -0.17 to 0.41. The new interpretation of this mode at 1xRMW is that substantial cooling occurs when there is a powerful hurricane with ample time to mix the upper ocean, translating over a thick barrier layer. This result supports the first part of *hypothesis three* in that hurricane parameters have a greater contribution to oceanic cooling closer to the hurricane

center. The second part of *hypothesis three* which states that oceanic parameters become more important for cooling further from the hurricane center is also supported by these results. At 4x, 3x, and 2xRMW, a shallow *ITLD* is the second most important mechanism for cooling, with loading values also indicating the presence of thin barrier layers. However, at 1xRMW, the *ITLD* becomes negligible, and the *BLT* seems to be opposite of what is conducive for cooling. The interpretation here is that a powerful hurricane with considerable time to generate upper ocean mixing is able to overcome a thick barrier layer in order to produce a large cooling response.

The same trends from mode 1 can be observed in mode 2, with 1xRMW exhibiting different results than 4x, 3x, and 2xRMW. At 4x, 3x, and 2xRMW, moderate cooling is seen in powerful hurricanes translating over a deep isothermal layers and thick barrier layers. The interpretation is that a powerful hurricane can overcome oceanic metrics not conducive for mixing (e.g., deep isothermal layer, large barrier layer) and still generate a cooling response. At 1xRMW, the loading value for ΔSST becomes negative, changing from 0.17 at 2xRMW to -0.29, indicating less of a cooling response. Additionally, loading values for hurricane parameter LU_h^{-1} and P_{min} become reduced (-0.01 and -0.18) in comparison to the oceanic parameters, *ITLD* and *BLT* with loading values of 0.91 and 0.24 respectively. These results indicate that slightly stronger hurricanes with average times to induce vertical mixing will have very little effect on oceanic cooling if there is an anomalously deep isothermal layer and a larger barrier layer beneath the hurricane. In opposition to mode 1, these results do not support *hypothesis three*. In moving closer to the hurricane center, hurricane parameters resulted in less cooling. Instead, the lack of response in ΔSST can be attributed to the presence of deep isothermal layers and larger barrier layers that restricted the ability for cool waters to be mixed up to the surface.

For mode 3 scores, 1xRMW also yielded different results compared to the other three datasets. At 4x, 3x, and 2xRMW, a negligible cooling response is observed, which can be attributed to large, positive loading values for *ITLD*, LU_h^{-1}, and *ITLD*. From these results, it can be inferred that even if a hurricane has a long time to generate upper ocean mixing, cooling will be minimal if the hurricane is weaker and translating over a deep isothermal layer. At 1xRMW, the loading value for ΔSST decreases from 0.05 to -0.23 indicating lower than average cooling responses. At 1xRMW, there is also a reversal of signs in the loading values for P_{min}, LU_h^{-1}, and *ITLD*, while the loading value for *BLT* increases significantly. These results mean that at 1xRMW, the presence of a strong hurricane over a shallow isothermal layer can yield lower than average cooling responses if the hurricane had minimal time to generate mixing, and was also translating over a large barrier layer.

Unlike modes 1, 2, and 3, mode 4 yields similar resulted in all four datasets. Within each, a negligible or minimal cooling response occurs, mainly due to a weak hurricane translating over a thick barrier layer. At 4x, 3x, and 2xRMW, however, results indicate considerably shallow isothermal layers. These results mean that even if a hurricane is translating over a shallow isothermal layer, cooling will be minimal if the hurricane is too weak and the barrier layer is thick. For 1xRMW, the loading value for *ITLD* becomes negligible, while the loading value for P_{min} increases. In a similar manner, this indicates that regardless of the *ITLD*, a weak hurricane translating over a thick barrier is unlikely to cause significant cooling.

As with mode 4, there were no major differences in loading values between the four datasets in mode 5. For this mode, very strong cooling is observed, although none of the loading values for the other four parameters are conducive for cooling. In all datasets, the loading values from this mode indicate substantial cooling occurring below weaker hurricanes with little time to

generate mixing that are translating over deep isothermal layers. Additionally, the thickness of the barrier layer is negligible in all four datasets.

Table 5: The loading values of each parameter for all five modes of the PCA from all four datasets.

	Parameter	Mode 1	Mode 2	Mode 3	Mode 4	Mode 5
4xRMW	*ΔSST*	0.64	0.21	0.04	0.11	0.73
	P_{min}	-0.31	-0.54	0.56	0.43	0.33
	LU_h^{-1}	0.47	0.13	0.73	-0.07	-0.47
	ITLD	-0.46	0.42	0.39	-0.58	0.35
	BLT	-0.24	0.68	0.05	0.68	-0.08
	Parameter	**Mode 1**	**Mode 2**	**Mode 3**	**Mode 4**	**Mode 5**
3xRMW	*ΔSST*	0.68	0.22	-0.01	0.02	0.70
	P_{min}	-0.23	-0.57	0.57	0.37	0.40
	LU_h^{-1}	0.51	0.09	0.69	-0.04	-0.51
	ITLD	-0.42	0.44	0.44	-0.59	0.30
	BLT	-0.21	0.66	0.10	0.72	-0.01
	Parameter	**Mode 1**	**Mode 2**	**Mode 3**	**Mode 4**	**Mode 5**
2xRMW	*ΔSST*	0.68	0.17	0.05	0.02	0.71
	P_{min}	-0.29	-0.63	0.36	0.49	0.39
	LU_h^{-1}	0.52	-0.11	0.65	0.11	-0.53
	ITLD	-0.38	0.32	0.66	-0.50	0.26
	BLT	-0.17	0.68	0.12	0.70	-0.03
	Parameter	**Mode 1**	**Mode 2**	**Mode 3**	**Mode 4**	**Mode 5**
1xRMW	*ΔSST*	0.57	-0.29	-0.23	-0.13	0.72
	P_{min}	-0.49	-0.18	-0.34	0.70	0.34
	LU_h^{-1}	0.51	-0.01	-0.58	0.33	-0.54
	ITLD	-0.02	0.91	-0.32	-0.06	0.27
	BLT	0.41	0.24	0.63	0.61	0.08

5.3 Discussion of Analysis of Variance on Oceanic cooling

Two ANOVA tests were completed on *ΔSST* to identify statistically significant differences in oceanic cooling between different months (Figure 21), as well as different hurricane categories (Figure 22). The ANOVA test binning by month yielded an insignificant p-value indicating that amount of oceanic cooling that occurs beneath hurricanes is not dependent on time of year. This result was present for data at 4x, 3x, 2x, and 1xRMW. Because SSTs

change considerably throughout the year with warmer temperatures in summer months and cooler temperatures in winter months, this result suggests that the pre-hurricane SST has little to no effect on the amount of cooling that occurs beneath a hurricane.

The ANOVA test binning by hurricane category, however, did yield a statistically significant result. Further analysis with a multiple comparisons test revealed that oceanic cooling is greater beneath category-2 hurricanes than category-1 hurricanes, with no other statistically significant differences among other categories. Previous studies (Haakman et al., 2019; Lloyd & Vecchi, 2011) have found similar results revealing that oceanic cooling increases considerably between category-1 and category-2 hurricanes with no differences in cooling between category-2 through category-5 hurricanes. One proposed explanation of this trend is the effect of the oceanic cooling feedback on hurricane intensity (Lloyd & Vecchi, 2011). In their paper, the authors suggest that water columns with strong stratification enhance cooling and act to suppress hurricane intensification, and conversely, water columns with weak stratification result in less overall cooling which supports hurricane intensification. As mentioned earlier, stratification is typically not conducive for cooling as it acts to inhibit vertical mixing which would limit the cooling response. However, when water columns are more stratified, there is generally a larger temperature difference between the surface and depth. Therefore, greater stratification coincides with larger temperature differences and larger transfers of heat from the surface to depth, resulting in a greater observed cooling at the surface. Lloyd & Vecchi (2011) argue that within their dataset, the observed oceanic cooling resulting from stratification and the enhanced vertical temperature gradient outweighed the reduction in vertical mixing and reduced cooling also brought on by stratification. This argument is supported by the ANOVA test, as well as the result

of the linear regression of N with ΔSST, which indicates that greater cooling occurs when N is larger, or when stratification is greater.

This information can then be used to potentially explain why no statistically significant differences occur in oceanic cooling beneath category-2 through category-5 hurricanes. In theory, regardless of stratification, category-1 hurricanes are not able to produce enough cooling to restrict themselves from intensifying to category-2. However, category-2 hurricanes translating over waters with strong stratification could be more likely to generate enough cooling to restrain themselves from intensifying into major hurricanes. Therefore, it is possible that major hurricanes are more likely to be present over weakly stratified water columns where cooling is suppressed as they would not be able to intensify into major hurricanes if they generated greater cooling. By that token, there are potentially some N and/or ΔSST thresholds beyond which intensification to subsequent hurricane categories is unable to be maintained. A direction of future work could be aimed at further exploring the effects of stratification, oceanic feedback, and potential parameter thresholds on hurricane intensification.

Lloyd and Vecchi (2011) also offer a second explanation in that category-2 hurricanes are strong enough to stir up the coldest waters. This implies that the waters stirred up to the surface by major hurricanes are of a similar temperature to those stirred up by category-2 hurricanes which would explain the similarities in ΔSST between category-2 through category-5 hurricanes. However, data from this study seem to support the former explanation over the latter. Figure 31 shows the scatter plot of V_{max} and ΔSST from the 2xRMW dataset, separated by hurricane category. Although the multiple comparisons test did not reveal statistically significant differences in ΔSST between category-2 through category-5 hurricanes, the scatter plot in Figure 31 still shows what appears to be a decreasing trend in ΔSST with increasing hurricane category

beginning with category-2. The mean *ΔSST* values for category-2, -3, -4, and -5 hurricanes are 1.8 ℃, 1.3 ℃, 1.3 ℃, and -0.4 ℃ respectively. Similarly, the maximum *ΔSST* values are 4.8 ℃, 3.1 ℃, 2 ℃, and -0.4 ℃. Though not statistically significant, these values imply less oceanic cooling in each subsequent category past category-2. If Lloyd & Vecchi's (2011) second explanation which stated that major hurricanes do not stir up colder waters than category-2 hurricanes were true, it would be expected that there would be no noticeable differences in *ΔSST* between category-2 through category-5 hurricanes. Therefore, the trends present in Figure 31 help support their first explanation that water column stratification and the feedback of oceanic cooling play a critical role in hurricane intensification beyond category-2, and that there is potentially some *N* and/or *ΔSST* threshold that cannot be exceeded for intensification to occur to subsequent hurricane categories. Future studies with more data on major hurricanes would be necessary to confirm or deny the existence of these trends.

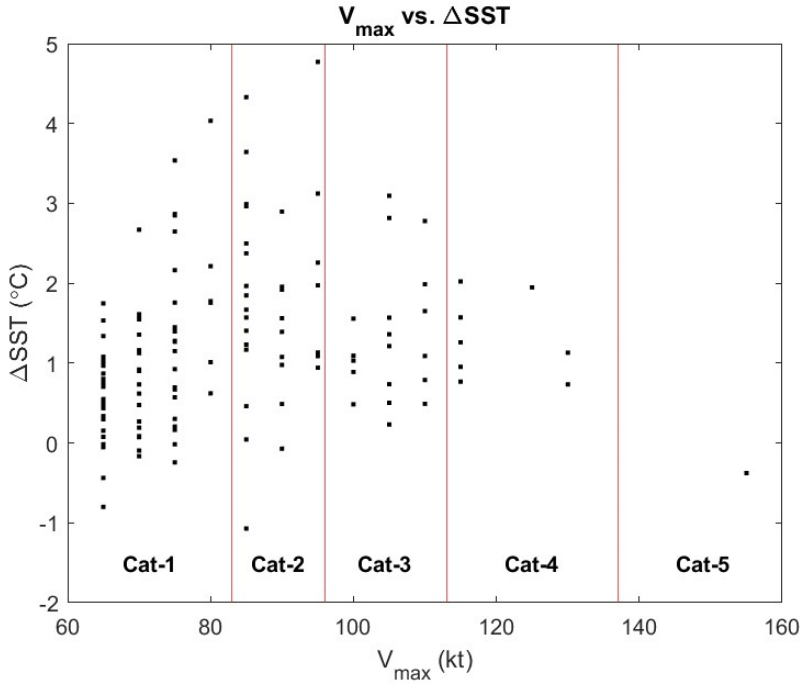

Figure 31: Scatter plot of V_{max} and ΔSST from the 2xRMW dataset. Red lines divide data points by hurricane category.

When binning *ΔSST* by hurricane category, the 1xRMW was the only data set in which there was no statistically significant difference in cooling between any two hurricane categories. 1xRMW. Figure 32 shows the box and whiskers plot of the ANOVA tests binning by hurricane category for at 4x, 3x, 2x, and 1xRMW. As with 2xRMW, there are statistically significant differences in *ΔSST* when using data for 4x and 3xRMW, with category-2 hurricanes resulting in greater cooling than category-1 hurricanes. However, for 1xRMW, there are no significant differences in cooling between any hurricane categories (p-value = 0.26). The interpretation of these results is that oceanic cooling close to the hurricanes center is not statistically different between hurricane categories, and that the cooling further from the hurricane center (4x, 3x, and 2xRMW) is statistically higher under category-2 hurricanes than under category-1 hurricanes. However, although the ANOVA test was not statistically significant at 1xRMW, the observed trend in Figure 32d is similar to those at 4x, 3x, and 2xRMW where the greatest cooling values are still occurring beneath category-2 hurricanes.

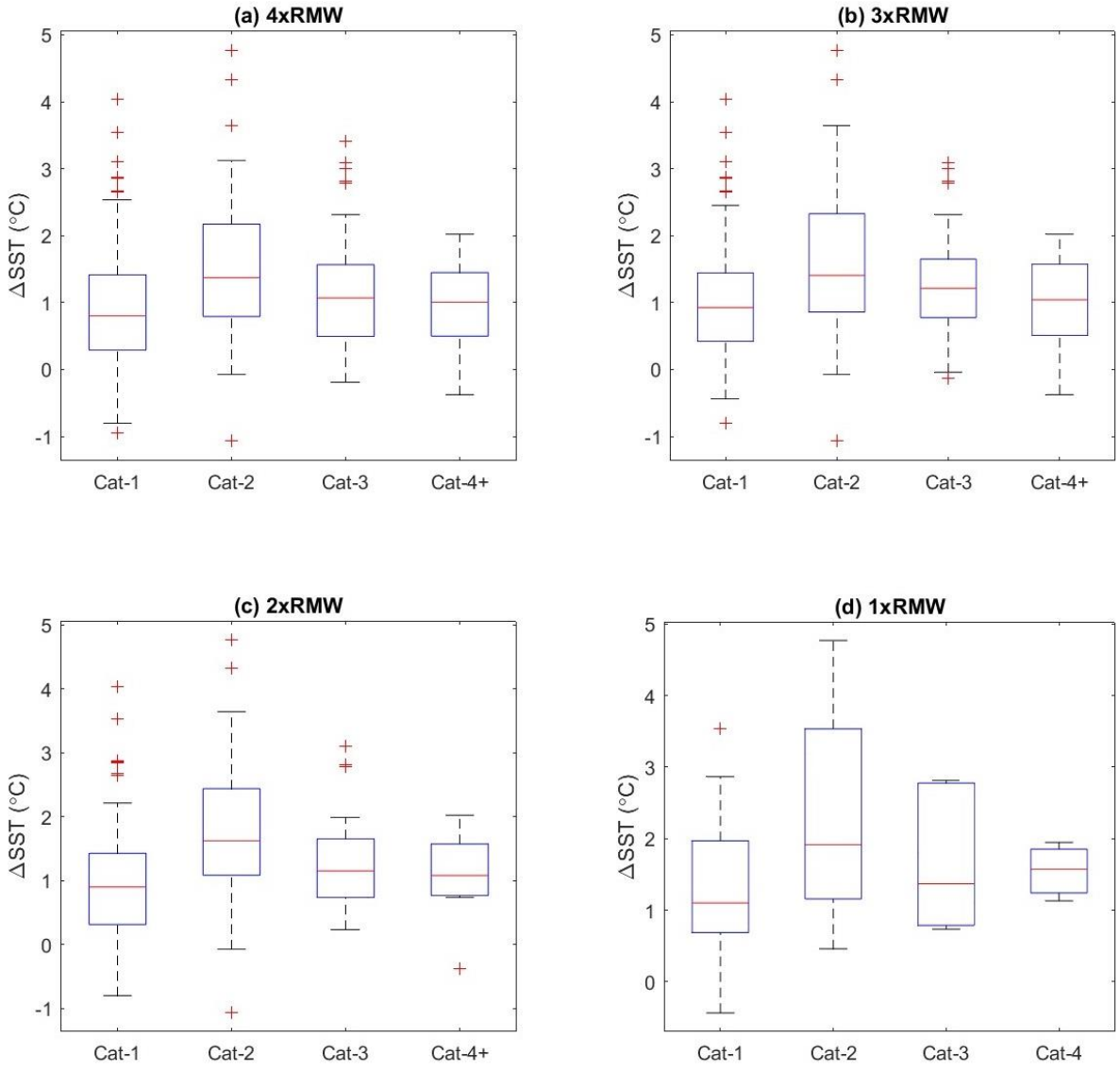

Figure 32: Box and whiskers plot for the results of the ANOVA test of ΔSST binning by hurricane category for (a) 4xRMW, p-value << 0.01, (b) 3xRMW, p-value << 0.01, (c) 2xRMW, p-value << 0.01, and (d) mode 4, p-value = 0.26. Red lines show the median cooling value for each month. Horizontal blue lines on each box represent the 25th and 75th percentile values. Horizontal black lines are maximum and minimum values that are not considered outliers. Red crosses are outlier values.

5.4 Discussion of Multilinear Regression

The final method of statistical analysis came in the form of MLR with the purpose of developing a MLR model that could explain the most variance in *ΔSST* using the fewest number

of parameters. The course of action was to use the parameters that had the greatest influence on ΔSST from the linear regressions and PCA, and develop MLR models with those until the addition of new parameters no longer explained more variance in ΔSST. Ultimately, a MLR model containing the three most influential parameters (LU_h^{-1}, P_{min}, and $ITLD$) was deemed best, explaining 32.1% of the variance in ΔSST. The addition of other parameters such as BLT, N, and Lat_{TC} led to a model that could explain only 0.3% more variance in ΔSST. The percentage of variance in ΔSST explained by the MLR models containing varying numbers of parameters is shown in Figure 23.

Figure 24 shows the scatter plot of ΔSST versus $\Delta SST_{predict}$ values. Based on the plot and differences between respective ΔSST and $\Delta SST_{predict}$ values, it can be noted that the parameters/mechanisms not considered in this study that influence ΔSST can not only enhance the cooling response, but also restrict it more than what is predicted by the MLR presented here. For instance, the maximum ΔSST value of 4.8 ℃ has an $\Delta SST_{predict}$ of 2.5 ℃. This cooling occurred beneath Hurricane Danielle (2010), which was a category-2 hurricane at that time with a V_{max} of 95 kt, P_{min} of 950 mbar, LU_h^{-1} of eight hours, while translating over an $ITLD$ of 23 m. Though each of these values are conducive for oceanic cooling, the predicted cooling is still over 2 ℃ less than the observed cooling. As such, unconsidered parameters not accounted for in this MLR model are still contributing to a considerable amount of cooling. The least amount of cooling was -1.1 ℃ (an SST increase of 1.1℃), associated with an $\Delta SST_{predict}$ is 0.7 ℃. This SST response also occurred beneath a category-2 hurricane, Hurricane Gordon (2006), at which point the system had a V_{max} of 85 kt, P_{min} of 972 mbar, LU_h^{-1} of three hours, while translating over an $ITLD$ of 51 m. Although these values are less conducive for cooling, a minimal cooling was still

expected based on the values for LU_h^{-1}, P_{min}, and *ITLD*. Opposite to the previous example, unaccounted for parameters here are actually reducing the SST response beneath the hurricane.

The mean difference between ΔSST and $\Delta SST_{predict}$ was relatively small at just 0.006 ℃ indicating that across the entirety of the dataset, the equation for $\Delta SST_{predict}$ provided by the MLR outputs similar values to observed ΔSST values. However, the larger standard deviation of 0.8 ℃ implies that while the statistical model may perform well on average, it is much less reliable if it were to be used to predict oceanic cooling beneath individual hurricanes. This furthers the argument for the importance of determining the other parameters/mechanisms that contribute to ΔSST, and including those in a statistical model that would yield low mean and standard deviation values of the difference between ΔSST and $\Delta SST_{predict}$. A statistical model with these results would allow for more reliable predictions of oceanic cooling on an individual level and could therefore be used to assist with hurricane intensity forecasts on an individual level as well.

As with the linear regressions, there was interest in understanding how the percentage of variance explained in ΔSST would change when analyzing data within varying ranges from the hurricane center. Following Figure 23, Figure 33 shows the percentage of variance in ΔSST explain by MLR models for each of the four datasets (4x, 3x, 2x, and 1xRMW). Within all four, the same trends exist in relation to explaining variance with in ΔSST. The combination of LU_h^{-1}, P_{min}, and *ITLD* tend to be able to explain roughly as much variance as the MLR models that also included *BLT*, *N*, and Lat_{TC}.

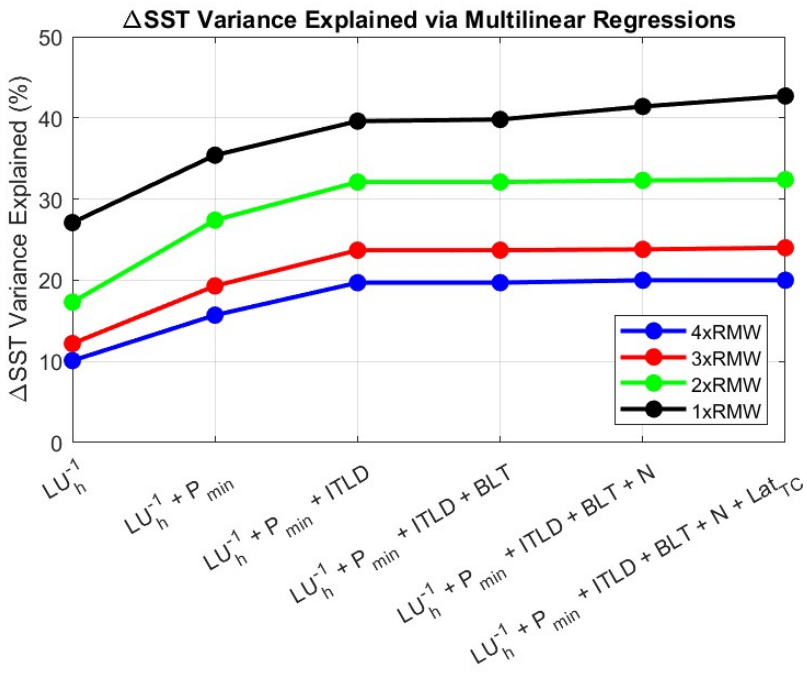

Figure 33: The percentage of variance explained in ΔSST from MLR models containing increasing numbers of predictor parameters for the four datasets.

The only dataset where some differences exist is 1xRMW in which there is a noticeable increase in the percentage of variance explained in ΔSST with the addition of both N and Lat_{TC} to the MLR. In the other datasets, differences between percentage of variance explained in ΔSST in the MLR containing all six parameters compared to those containing just LU_h^{-1}, P_{min}, and $ITLD$ are all 0.3%. In comparison, the difference at 1xRMW is 3.1%. The reasoning behind this sudden increase could possibly be explained by the p-values and r^2 values associated with the 1xRMW presented in Table 3. Although parameters at 1xRMW saw the highest r^2 values, several of the linear regressions that were statistically significant at 4x, 3x, and 2xRMW now had p-values greater than 0.05. Thus, increased r^2 values associated with the 1xRMW may not be statistically significant and should be noted when interpreting these results. Furthermore, while the 3.1% increase is greater than the 0.3% increase in the other datasets, it is still relatively small in regard

to the variance explained by LU_h^{-1}, P_{min}, and *ITLD*. In an ideal scenario, more data collected at 1xRMW would give a better sense of the true trends that exist between the parameters examined through this project with *ΔSST* within 1xRMW.

Trends at 4xRMW down to 1xRMW support *hypothesis three* in that there would be improvements in the statistics (more variance explained in *ΔSST*) when using data concentrated closer to the hurricane center. This was the expected result because at some distance from the storm center, the hurricane will have no effect on the ocean surface. As such, the datasets containing data furthest from the hurricane center (e.g., 4xRMW) would be expected to explain less variance in *ΔSST* compared to those where data is concentrated close to the hurricane center (e.g., 1xRMW). Focusing on the MLRs from each dataset that contain just LU_h^{-1}, P_{min}, and *ITLD*, it can be seen that the difference in variance explained in *ΔSST* differs from dataset to dataset. The smallest gap in the percentage of variance explained in *ΔSST* is from 4xRMW to 3xRMW, where there is an increase of 4%. Comparatively, the percentages of variance explained in *ΔSST* from 3xRMW to 2xRMW, and 2xRMW to 1xRMW are 8.4% and 7.5% respectively. The substantial increase in the variance explained in *ΔSST* supports earlier arguments that data closest to the hurricane center is best for the prediction of *ΔSST*, and that data outside of 2xRMW should be avoided if possible as there is a considerable drop off in the variance explained between 3xRMW and 2xRMW. The impact of hurricanes on oceanic cooling is more predictable when data is taken from within the *RMW*, and becomes increasingly less predictable when data further from the hurricane center is used.

6. CONCLUSION

6.1 Summary of Project

The overarching goal of this project was to further the understanding of the parameters contributing to hurricane-induced oceanic cooling (*ΔSST*). To accomplish this, 17 years of observational hurricane and oceanic data from 2003 through 2019 in the North Atlantic basin were analyzed using a wide range of statistical analyses. Hurricane data for this project were obtained from CSU's EBTRK dataset. EBTRK is an expansive hurricane dataset that serves as an extension of NOAA's HURDAT2 dataset by containing additional parameters. The majority of oceanic data were derived from Argo float profiles that were matched with hurricane observation points so that the oceanic data from the Argo float profiles resembled ocean conditions just prior to and in the vicinity of the hurricanes. The remaining oceanic parameter, *ΔSST,* was calculated using satellite sea surface temperatures from NASA's JPL's GHRSST Level 4 SST analysis product.

Every hurricane observation point has a single value for each parameter in EBTRK. After the matching process of hurricane observation points and Argo float profiles, and the calculation of *ΔSST,* a dataset was constructed where each hurricane observation point contained its single values for hurricane parameters, single values for the oceanic parameters from its matched Argo float profile, and a single value for *ΔSST*. Three other datasets were then created based on the original dataset. The matching process for the original dataset required Argo float profiles to be within a distance of four times the radius of maximum winds of a hurricane. The three new datasets included all the data the Argo float profile was within three times the radius of

maximum winds, two times the radius of maximum winds, and one times the radius of maximum winds respectively.

The first method of statistical analysis was linear regression. Linear regressions were run on ΔSST against each of the remaining hurricane and oceanic parameters to identify those with statistically significant relationships with ΔSST, and how much variance in ΔSST they could explain. The second method was principal component analysis. This was done to identify parameters that may work in tandem to contribute to oceanic cooling. The third method of statistical analysis was analysis of variance, done to identify statistically significant differences in oceanic cooling across hurricane category and month. Analysis of variance was also performed on mode scores from the principal component analysis to identify whether there were statistically significant differences in mode scores across different months. The spatial distribution of mode scores were also plotted to identify any trends that existed within the basin. The fourth and final method of statistical analysis was multilinear regression. Based on results from the first three method of statistical analysis, several multilinear regression models were developed to identify the fewest number of parameters that could explain the most variance in ΔSST.

The primary takeaway from this study is that hurricane parameters have a greater influence on ΔSST than oceanic parameters. In particular, the time available for vertical mixing LU_h^{-1} has the greatest influence on the observed cooling response, with higher values (more time) resulting in greater cooling. LU_h^{-1} is a function of two hurricane parameters, translation speed U_h and size, defined by the radius of maximum winds RMW. Through linear regressions of these individual parameters with ΔSST, it is apparent that a hurricane's U_h is the dominant of the two. Thus, the single parameter with the greatest impact on ΔSST is U_h. However, taking RMW

into account through the calculation of LU_h^{-1} results in greater variance explained in ΔSST making it a more ideal metric. Following LU_h^{-1}, hurricane strength as a function of minimum sea level pressure P_{min} is the next most important parameter contributing to ΔSST, with lower values (stronger hurricanes) resulting in greater cooling. Of those considered, the oceanic metric that contributed the most to ΔSST is the isothermal layer depth *ITLD*, with lower values (shallower isothermal layers) resulting in greater cooling. These results, as well as those from the PCA support *hypothesis one* and *hypothesis two* in that the greatest cooling response is likely to occur under powerful hurricanes translating over shallow isothermal layers with ample time to generate mixing in the upper ocean. While hurricane parameters LU_h^{-1} and P_{min} may be the most important for predicting ΔSST, results from the PCA also emphasize the importance of taking oceanic parameters into consideration under particular circumstances if possible, as hurricane strength and time to generate vertical mixing can be restricted by the depth of the isothermal layer and/or the thickness of the barrier layer.

Results from this study also generally support the first part of *hypothesis three* in that hurricane parameters have a greater impact on ΔSST closer to the hurricane center. Results from the linear regressions and MLRs indicate hurricane parameters LU_h^{-1} and P_{min} explain greater variance in ΔSST in each subsequent dataset (4x, 3x, 2x, and 1xRMW). However, the second part of *hypothesis three*, which states that oceanic parameters become more important to ΔSST further from the hurricane center, is not supported by this study. There is no clear or significant trend in the contribution of the *ITLD*, isopycnal layer depth *IPLD*, barrier layer thickness *BLT*, or Brunt-Vaisala frequency *N* with ΔSST at 4x, 3x, 2x, and 1xRMW.

6.2 Future Work

There are a few directions that can be taken based up previous work and the results of this study. One direction would be identifying the relative importance of different parameters to oceanic cooling across different ocean basins. In attempting to predict the oceanic cooling beneath hurricanes, it would be beneficial to understand how these statistics vary in different parts of the world. As seen here, LU_h^{-1}, P_{min}, and *ITLD* appear to be three most important parameters to the cooling response beneath North Atlantic hurricanes. Is this the same case in the western Pacific and Indian Oceans? Similarly, it is of interest to determine how the relative importance of these parameters vary within the same basin (e.g., Gulf of Mexico vs. Caribbean Sea vs. western North Atlantic).

Another question is how strong is the relationship between oceanic cooling and differences in hurricane intensification? Other directions of interest involve the effects of a warming climate on hurricane strength, hurricane frequency, and ocean temperatures. How will the cooling response observed beneath hurricanes change with the warming climate? How will this impact the feedback of cold wakes on hurricane intensity? If ocean temperatures rise but cooling responses remain at similar levels, will the effect on hurricane intensity not be as strong as long as ocean temperatures are warm enough to support intensification?

Lastly, what other parameters/mechanisms can be used to predict oceanic cooling? Based on the MLRs presented here, the parameters identified in this study are able to explain ~32% of the variance in oceanic cooling. What other hurricane or oceanic metrics could be impacting oceanic cooling that are not taken into consideration in this study? One metric that could be of interest is the TCHP. Introduced by Whitaker (1967), TCHP is an oceanic metric that can be described as the vertical integration of temperature within the water column above the 26 °C

isotherm (Potter et al., 2019). As mentioned earlier, a general rule of thumb is that hurricanes require ocean temperatures of at least 26 ℃ in order for heat fluxes to remain at levels that can support hurricane intensification (Palmen, 1948; D'Asaro et al., 2007). TCHP is typically used to assist with predictions of hurricane intensification, though maybe a relationship exists between itself and *ΔSST*, or the depth of the 26 ℃ isotherm and *ΔSST*. Another oceanic parameter that could be of interest is the barrier layer potential energy (BLPE). In their 2019 paper, Haakman and authors and used just two oceanic metrics, *BLT* and BLPE when studying cold wakes in the North Atlantic Ocean, with BLPE outperforming *BLT* in regard to hurricane-induced oceanic cooling. *BLPE* has been put forth as a better metric than *BLT* because it allows for a better insight into differences in stratification between the surface and *ITLD* (Chi et al., 2014). With *BLT* producing no statistically significant results in this study, the use of BLPE could potentially produce more insightful results in future work.

REFERENCES

1. Babin, S. M., Carton, J. A., Dickey, T. D., & Wiggert, J. D. (2004). Satellite evidence of hurricane-induced phytoplankton blooms in an oceanic desert. *Journal of Geophysical Research: Oceans*, *109*(C3).
2. Bates, N. R., Knap, A. H., & Michaels, A. F. (1998). Contribution of hurricanes to local and global estimates of air–sea exchange of CO2. *Nature*, *395*(6697), 58-61.
3. Bates, N. R., Takahashi, T., Chipman, D. W., & Knap, A. H. (1998). Variability of pCO2 on diel to seasonal timescales in the Sargasso Sea near Bermuda. *Journal of Geophysical Research: Oceans*, *103*(C8), 15567-15585.
4. Bender, M. A., Ginis, I., & Kurihara, Y. (1993). Numerical simulations of tropical cyclone-ocean interaction with a high-resolution coupled model. *Journal of Geophysical Research: Atmospheres*, *98*(D12), 23245-23263.
5. Biogeochemical Argo. (2021). "General Context." Retrieved from https://biogeochemical-argo.org/scientific-questions-general-context.php
6. Bjarnadottir, S., Li, Y., & Stewart, M. G. (2011). A probabilistic-based framework for impact and adaptation assessment of climate change on hurricane damage risks and costs. *Structural Safety*, *33*(3), 173-185.
7. Born, G. H., Dunne, J. A., & Lame, D. B. (1979). Seasat mission overview. *Science*, *204*(4400), 1405-1406.
8. Cangialosi, J. P., & Franklin, J. L. (2012). National Hurricane Center forecast verification report. *National Hurricane Center (NHC)*, *79*.

9. Cangialosi, J. P., Blake, E., DeMaria, M., Penny, A., Latto, A., Rappaport, E., & Tallapragada, V. (2020). Recent progress in tropical cyclone intensity forecasting at the National Hurricane Center. *Weather and Forecasting*, *35*(5), 1913-1922.
10. Chan, J. C. L., & Gray, W. M. (1982). Tropical cyclone movement and surrounding flow relationships. *Monthly Weather Review*, *110*(10), 1354-1374.
11. Chan, J. C. L. (1982). *On the physical processes responsible for tropical cyclone motion*. Diss. Colorado State University.
12. Chan, K. T., & Chan, J. C. (2012). Size and strength of tropical cyclones as inferred from QuikSCAT data. *Monthly weather review*, *140*(3), 811-824.
13. Chang, S. W., & Anthes, R. A. (1978). Numerical simulations of the ocean's nonlinear, baroclinic response to translating hurricanes. *Journal of Physical Oceanography*, *8*(3), 468-480.
14. Chi, N. H., Lien, R. C., D'Asaro, E. A., & Ma, B. B. (2014). The surface mixed layer heat budget from mooring observations in the central Indian Ocean during Madden–Julian Oscillation events. *Journal of Geophysical Research: Oceans*, *119*(7), 4638-4652.
15. Chiang, T. L., Wu, C. R., & Oey, L. Y. (2011). Typhoon Kai-Tak: An ocean's perfect storm. *Journal of Physical Oceanography*, *41*(1), 221-233.
16. Cione, J. J., & Uhlhorn, E. W. (2003). Sea surface temperature variability in hurricanes: Implications with respect to intensity change. *Monthly Weather Review*, *131*(8), 1783-1796.
17. Collins III, C. O., Potter, H., Lund, B., Tamura, H., & Graber, H. C. (2018). Directional wave spectra observed during intense tropical cyclones. *Journal of Geophysical Research: Oceans*, *123*(2), 773-793.

18. Dare, R. A., & McBride, J. L. (2011). Sea surface temperature response to tropical cyclones. *Monthly Weather Review*, *139*(12), 3798-3808.
19. D'Asaro, E. A., Sanford, T. B., Niiler, P. P., & Terrill, E. J. (2007). Cold wake of hurricane Frances. *Geophysical Research Letters*, *34*(15).
20. DeMaria, M., Sampson, C. R., Knaff, J. A., & Musgrave, K. D. (2014). Is tropical cyclone intensity guidance improving?. *Bulletin of the American Meteorological Society*, *95*(3), 387-398.
21. Diaz, B. P., Knowles, B., Johns, C. T., Laber, C. P., Bondoc, K. G. V., Haramaty, L., Natale, F., Harvey, E. L., Kramer, S. J., Bolaños, L. M., Lowenstein, D. P., Fredericks, H. F., Graff, J., Westberry, T. K., Mojica, K. D. A., Haëntjens, N., Nicholas, B., Gaube, P., Boss, E., Carlson, C. A., Behrenfield, M. J., Van Mooy, B. A. S., & Bidle, K. D. (2021). Seasonal mixed layer depth shapes phytoplankton physiology, viral production, and accumulation in the North Atlantic. *Nature communications*, *12*(1), 1-16.
22. Dvorak, V. F. (1975). Tropical cyclone intensity analysis and forecasting from satellite imagery. *Monthly Weather Review*, *103*(5), 420-430.
23. Emanuel, K. A. (1986). An air-sea interaction theory for tropical cyclones. Part I: Steady-state maintenance. *Journal of Atmospheric Sciences*, *43*(6), 585-605.
24. Emanuel, K. (2001). Contribution of tropical cyclones to meridional heat transport by the oceans. *Journal of Geophysical Research: Atmospheres*, *106*(D14), 14771-14781.
25. Emanuel, K. (2003). Tropical cyclones. *Annual review of earth and planetary sciences*, *31*(1), 75-104.
26. Foltz, G. R., & McPhaden, M. J. (2009). Impact of barrier layer thickness on SST in the central tropical North Atlantic. *Journal of Climate*, *22*(2), 285-299.

27. Frank, W. M., & Ritchie, E. A. (2001). Effects of vertical wind shear on the intensity and structure of numerically simulated hurricanes. *Monthly weather review*, *129*(9), 2249-2269.

28. Franklin, J. L., Black, M. L., & Valde, K. (2003). GPS dropwindsonde wind profiles in hurricanes and their operational implications. *Weather and Forecasting*, *18*(1), 32-44.

29. Galarneau, T. J., & Davis, C. A. (2013). Diagnosing forecast errors in tropical cyclone motion. *Monthly weather review*, *141*(2), 405-430.

30. GHRSST Science Team (2010), The Recommended GHRSST Data Specification (GDS) 2.0, document revision 4, available from the GHRSST International Project Office, 2011, pp 123.

31. Ginis, I. (2002). Tropical cyclone-ocean interactions. Atmosphere-Ocean Interactions. *Advances in Fluid Mechanics Series*, *1*(33), 83-114.

32. Gonella, J. (1972). A rotary-component method for analysing meteorological and oceanographic vector time series. *Deep Sea Research and Oceanographic Abstracts*, 19(12), 833-846.

33. Gray, William M. (1975). *Tropical cyclone genesis*. Diss. Colorado State University.

34. Greatbatch, R. J. (1985). On the role played by upwelling of water in lowering sea surface temperatures during the passage of a storm. *Journal of Geophysical Research: Oceans*, *90*(C6), 11751-11755.

35. Gruber, N., Clement, D., Carter, Feely, B. R., Van Heuven, S., Hoppema, M., Ishii, M., Key, R. M., Kozyr, A., Lauvset, S. K., Lo Monaco, C., Mathis, J. T., Murata, A., Olsen, A., Perez, F. F., Sabine, C. L., Tanhua, T., & Wanninkhof, R. (2019). The oceanic sink for anthropogenic CO2 from 1994 to 2007. *Science*, *363*(6432), 1193-1199.

36. Haakman, K., Sayol, J. M., van der Boog, C. G., & Katsman, C. A. (2019). Statistical characterization of the observed cold wake induced by North Atlantic hurricanes. *Remote Sensing*, *11*(20), 2368.

37. Halverson, J. B., Simpson, J., Heymsfield, G., Pierce, H., Hock, T., & Ritchie, L. (2006). Warm core structure of Hurricane Erin diagnosed from high altitude dropsondes during CAMEX-4. *Journal of the atmospheric sciences*, *63*(1), 309-324.

38. Houze Jr, R. A., Chen, S. S., Smull, B. F., Lee, W. C., & Bell, M. M. (2007). Hurricane intensity and eyewall replacement. *Science*, *315*(5816), 1235-1239.

39. IPCC, 2018: Global Warming of 1.5°C.An IPCC Special Report on the impacts of global warming of 1.5°C above pre-industrial levels and related global greenhouse gas emission pathways, in the context of strengthening the global response to the threat of climate change, sustainable development, and efforts to eradicate poverty [Masson-Delmotte, V., P. Zhai, H.-O. Pörtner, D. Roberts, J. Skea, P.R. Shukla, A. Pirani, W. Moufouma-Okia, C. Péan, R. Pidcock, S. Connors, J.B.R. Matthews, Y. Chen, X. Zhou, M.I. Gomis, E. Lonnoy, T. Maycock, M. Tignor, and T. Waterfield (eds.)]. In Press.

40. Jayne, S.R., D. Roemmich, N. Zilberman, S.C. Riser, K.S. Johnson, G.C. Johnson, and S.R. Piotrowicz. 2017. The Argo Program: Present and future. *Oceanography*, *30*(2), 18–28.

41. Jordan, C. L., & Frank, N. L. (1964). On the influence of tropical cyclones on the sea surface temperature field, in Proceedings of Symposium On Tropical Meteorology, pp. 614–622, N. Z. Meteorol. Serv., Wellington.

42. JPL MUR MEaSUREs Project. 2015. GHRSST Level 4 MUR Global Foundation Sea Surface Temperature Analysis. Ver. 4.1. PO.DAAC, CA, USA. Dataset accessed at https://doi.org/10.5067/GHGMR-4FJ04

43. Kanada, S., Tsujino, S., Aiki, H., Yoshioka, M. K., Miyazawa, Y., Tsuboki, K., & Takayabu, I. (2017). Impacts of SST patterns on rapid intensification of Typhoon Megi (2010). *Journal of Geophysical Research: Atmospheres*, *122*(24), 13-245.

44. Karnauskas, K. B., Zhang, L., & Emanuel, K. A. (2021). The feedback of cold wakes on tropical cyclones. *Geophysical Research Letters*, *48*(7), e2020GL091676.

45. Kelly, K. A., & Qiu, B. (1995). Heat flux estimates for the western North Atlantic. Part I: Assimilation of satellite data into a mixed layer model. *Journal of physical oceanography*, *25*(10), 2344-2360.

46. Kishore, N., Marqués, D., Mahmud, A., Kiang, M. V., Rodriguez, I., Fuller, A., Ebner, P., Sorensen, C., Racy, F., Lemery, L., Maas, L., Leaning, J., Irizarry, R. A., Balsari, S., & Buckee, C. (2018). Mortality in Puerto Rico after hurricane maria. *New England journal of medicine*, *379*(2), 162-170.

47. Knabb, R. D., Rhome, J. R., and Brown, D. P. Tropical Cyclone Report Hurricane Katrina 23-30 August 2005. National Hurricane Center. 2005.

48. Koch, J., McKinley, G. A., Bennington, V., & Ullman, D. (2009). Do hurricanes cause significant interannual variability in the air-sea CO2 flux of the subtropical North Atlantic?. *Geophysical Research Letters*, *36*(7).

49. Kossin, J. P. (2018). A global slowdown of tropical-cyclone translation speed. *Nature*, *558*(7708), 104-107.

50. Landsea, C. W. and Franklin, J. L., 2013: Atlantic Hurricane Database Uncertainty and Presentation of a New Database Format. *Monthly Weather Review*, *141*(10), 3576-3592.
51. Lawrence, M. B., and Cobb, H. D. Tropical Cyclone Report Hurricane Jeanne 13-28 September 2004. National Hurricane Center. 2005.
52. Lloyd, I. D., & Vecchi, G. A. (2011). Observational evidence for oceanic controls on hurricane intensity. *Journal of Climate*, *24*(4), 1138-1153.
53. Mao, Q., Chang, S. W., & Pfeffer, R. L. (2000). Influence of large-scale initial oceanic mixed layer depth on tropical cyclones. *Monthly weather review*, *128*(12), 4058-4070.
54. Maurer, J. (2002). Infrared and microwave remote sensing of sea surface temperature (SST). *University of Hawai'i*.
55. Mei, W., & Pasquero, C. (2013). Spatial and temporal characterization of sea surface temperature response to tropical cyclones. *Journal of Climate*, *26*(11), 3745-3765.
56. Michaels, P. J., Knappenberger, P. C., & Davis, R. E. (2006). Sea-surface temperatures and tropical cyclones in the Atlantic basin. *Geophysical Research Letters*, *33*(9).
57. Miller, J. R. (1976). The salinity effect in a mixed layer ocean model. *Journal of Physical Oceanography*, *6*(1), 29-35.
58. Mitchell, J. F. (1989). The "greenhouse" effect and climate change. *Reviews of Geophysics*, *27*(1), 115-139.
59. Murty, T. S., & Neralla, V. R. (1992). On the recurvature of tropical cyclones and the storm surge problem in Bangladesh. *Natural Hazards*, *6*(3), 275-279.
60. NOAA AOML PhOD. "What is Argo?" Retrieved from https://www.aoml.noaa.gov/phod/argo/webpage_sections/doc/argo_intro_what_is.php

61. Obata, A., Ishizaka, J., & Endoh, M. (1996). Global verification of critical depth theory for phytoplankton bloom with climatological in situ temperature and satellite ocean color data. *Journal of Geophysical Research: Oceans*, *101*(C9), 20657-20667.

62. Palmen, E. (1948). On the formation and structure of tropical hurricanes. *Geophysica*, *3*(1), 26-38.

63. Pasch, R. J., Avila, L. A., & Jiing, J. G. (1998). Atlantic tropical systems of 1994 and 1995: A comparison of a quiet season to a near-record-breaking one. *Monthly Weather Review*, *126*(5), 1106-1123.

64. Potter, H., Drennan, W. M., & Graber, H. C. (2017). Upper oceanic cooling and air-sea fluxes under typhoons: A case study. *Journal of Geophysical Research: Oceans*, *122*(9), 7237-7252.

65. Potter, H., DiMarco, S. F., & Knap, A. H. (2019). Tropical cyclone heat potential and the rapid intensification of Hurricane Harvey in the Texas Bight. *Journal of Geophysical Research: Oceans*, *124*(4), 2440-2451.

66. Potter, H., & Rudzin, J. E. (2021). Upper-ocean temperature variability in the Gulf of Mexico with implications for hurricane intensity. *Journal of Physical Oceanography*, *51*(10), 3149-3162.

67. Price, J. F. (1981). Upper ocean response to a hurricane. *Journal of Physical Oceanography*, *11*(2), 153-175.

68. Price, J. F., Weller, R. A., & Pinkel, R. (1986). Diurnal cycling: Observations and models of the upper ocean response to diurnal heating, cooling, and wind mixing. *Journal of Geophysical Research: Oceans*, *91*(C7), 8411-8427.

69. Rosendal, H. E., & Shaw, S. L. (1982). Relationship of maximum sustained winds to minimum sea level pressure in central north pacific tropical cyclones. *NOAA Technical Memorandum NWSTM PR-24.*

70. Sarmiento & Gruber. (2006). Air-Sea Interface. *Ocean Biogeochemical Dynamics*. (pp. 73-101). Princeton, NJ. Princeton University Press.

71. Schade, L. R., & Emanuel, K. A. (1999). The ocean's effect on the intensity of tropical cyclones: Results from a simple coupled atmosphere–ocean model. *Journal of the Atmospheric Sciences, 56*(4), 642-651.

72. Shay, L. K., Goni, G. J., & Black, P. G. (2000). Effects of a warm oceanic feature on Hurricane Opal. *Monthly Weather Review, 128*(5), 1366-1383.

73. Shultz, J. M., Russell, J., & Espinel, Z. (2005). Epidemiology of tropical cyclones: the dynamics of disaster, disease, and development. *Epidemiologic reviews*, *27*(1), 21-35.

74. Sitkowski, M., Kossin, J. P., & Rozoff, C. M. (2011). Intensity and structure changes during hurricane eyewall replacement cycles. *Monthly Weather Review, 139*(12), 3829-3847.

75. Smith, R. K. (1980). Tropical cyclone eye dynamics. *Journal of Atmospheric Sciences, 37*(6), 1227-1232.

76. Spall, M. A. (1991). A diagnostic study of the wind-and buoyancy-driven North Atlantic circulation. *Journal of Geophysical Research: Oceans*, *96*(C10), 18509-18518.

77. Sriver, R. L., & Huber, M. (2007). Observational evidence for an ocean heat pump induced by tropical cyclones. *Nature, 447*(7144), 577-580.

78. Stull, R. (2011). Stability. *Meteorology for Scientists and Engineers, 3rd Edition* (pp. 119-158). The University of British Columbia. isbn 978-0-88865-178-5**.**

79. Thomson, R. E., & Fine, I. V. (2003). Estimating mixed layer depth from oceanic profile data. *Journal of Atmospheric and Oceanic Technology*, *20*(2), 319-329.

80. Thorncroft, C. D., & Hoskins, B. J. (1994). An idealized study of African easterly waves. I: A linear view. *Quarterly Journal of the Royal Meteorological Society*, *120*(518), 953-982.

81. Tomiyasu, K. (1974). Remote sensing of the earth by microwaves. *Proceedings of the IEEE*, *62*(1), 86-92.

82. Vigh, Jonathan L. (2010). *Formation of the hurricane eye*. Diss. Colorado State University.

83. Wang Bin, R. L., Yuqing, W., & Liguang, W. (1999). Dynamics in tropical cyclone motion: A review. *Chinese Journal of Atmospheric Sciences*, *22*(4), 416-434.

84. Wang, X., Han, G., Qi, Y., & Li, W. (2011). Impact of barrier layer on typhoon-induced sea surface cooling. *Dynamics of Atmospheres and Oceans*, *52*(3), 367-385.

85. Wendland, W. M. (1977). Tropical storm frequencies related to sea surface temperatures. *Journal of Applied Meteorology (1962-1982)*, 477-481.

86. Whitaker, W. D. (1967). *Quantitative determination of heat transfer from sea to air during passage of Hurricane Betsy*. Diss. Texas A&M University.

87. Wong, A., Keeley, R., & Carval, T., Argo Data Management Team. (2013). Argo Quality Control Manual (Version 2.8) [PDF file]. Retrieved from http://www.argodatamgt.org/content/download/15699/102401/file/argo-quality-control-manual-version2.8.pdf

88. Yablonsky, R. M., & Ginis, I. (2012). Impact of a warm ocean eddy's circulation on hurricane-induced sea surface cooling with implications for hurricane intensity. *Monthly weather review*, *141*(3), 997-1021.

89. Zhang, J., Lin, Y., Chavas, D. R., & Mei, W. (2019). Tropical cyclone cold wake size and its applications to power dissipation and ocean heat uptake estimates. *Geophysical Research Letters*, *46*(16), 10177-10185.

90. Zhang, Y., Xu, H., Qiao, F., & Dong, C. (2018). Seasonal variation of the global mixed layer depth: comparison between Argo data and FIO-ESM. *Frontiers of earth science*, *12*(1), 24-36.